

July 1, 1971

FINAL REPORT (II)
RESEARCH IN THE DEVELOPMENT
OF AN
IMPROVED MULTIPLIER PHOTOTUBE

Contract NASW-1855
Department of Astronomy Programs
National Aeronautics and Space Administration

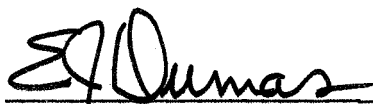
Period Covered:
July 1970 - July 1971

Prepared by:

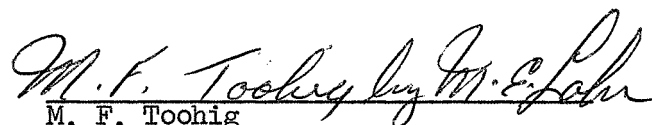
H. W. Baker, E. H. Eberhardt, and R. J. Hertel

International Telephone and Telegraph Corporation
Tube and Sensor Laboratories
3700 East Pontiac Street
Fort Wayne, Indiana

Approved by:



E. J. Dumas
E. J. Dumas
Manager, Applied Research and
Photosensor Laboratories



M. F. Toohig
M. F. Toohig
Vice President and General Manager
Tube and Sensor Laboratories

TABLE OF CONTENTS

	Page
1.0 INTRODUCTION	1
2.0 PROGRAM OBJECTIVES	1
3.0 SUMMARY OF RESULTS	2
3.1 Program A (Non-scanned photomultipliers)	2
3.2 Program B (Image intensifier dissectors)	2
4.0 LOW LEVEL FLUX SOURCE	4
4.1 Photomultiplier tests	4
4.2 Smoothing Dissector Tests.	5
5.0 THEORY OF SMOOTHING.	6
6.0 FREQUENCY RESPONSE	8
7.0 LINEARITY	14
8.0 S/N RATIO	17
9.0 PERFORMANCE AS A SPECTRUM SCANNER	25
9.1 Single Electron Counting Characteristics	31
9.2 Single Electron Scintillations	34
10.0 SPECTRAL RESPONSE MEASUREMENTS	37
11.0 MEETINGS AND DISCUSSIONS	39
12.0 GENERAL CONCLUSIONS.	39
13.0 REFERENCES	40
14.0 APPENDICES	41
A. Applications Note E17.	41
B. Technical Note 115.	42
C. Dissector S/N Ratio	43

1.0 INTRODUCTION

This report covers the work done on the 1 year extension of Contract NASW-1855. The first year's work was reported in Final Report, IIT-ETD 70-006, Project 11-23700, May 21, 1970.

Three quarterly reports, (the 5th 6th and 7th quarterlies) have already been issued. Their results are included in (or are summarized in) this final report.

2.0 PROGRAM OBJECTIVES

Program A: (Non-scanned Photomultipliers)

A-1 Improve the accuracy of our absolute quantum counting measurements.

A-2 Correlate the measured single electron pulse height spectrum with analogue noise current measurements.

A-3 Determine the dynamic range of pulse counting rates on fast (F4034) photomultiplier tubes.

A-4 Investigate the stabilization time requirements in photomultiplier tubes.

A-5 Discuss our test results with interested astronomers and consign tubes for test as feasible.

Program B: (Image Intensifier Dissectors)

B-1 Measure the overall quantum counting efficiency of an image intensifier dissector.

B-2 Correlate measured counting efficiency with expected behavior.

B-3 Compare dissector counting behavior with and without image intensifier preamplifier.

B-4 Determine the time "smear" characteristics of phosphor screens under single electron excitation.

B-5 Discuss our test results with interested astronomers and consign tubes for test as feasible.

3.0 SUMMARY OF RESULTS

3.1 Program A (Non-scanned photomultipliers)

Effort on this program was confined to the establishment of a calibrated flux source using "neutral" density low levels (a few photons/cm²/sec), (reported in Section 4.0 below). Further effort on Program A was curtailed in view of the intense interest in Program B, and the resultant possibility of assisting in a substantial "break through" in the art of astronomical detectors.

3.2 Program B (Image Intensifier Dissectors)

Many of the basic questions regarding smoothing dissectors (image intensifier image dissector modules) were investigated on this program:

(a) The detection properties of one and two stage tubes were compared to dissectors alone.

(b) The nature of the phosphor decay time at very low excitation levels (below the visible level) were measured.

(c) The smoothing dissector was shown to be a distinct improvement (30 to 90 times) over a scanned photomultiplier (i.e. an image dissector).

(d) Performance was checked in both the single electron counting and the current-measuring modes of operation, with equivalent improvements observed.

(e) Anomalously superior performance was observed at slow scan rates, indicating a need for further experimental and analytical efforts.

(f) A technical paper describing our results was prepared, and has been accepted for publication in Applied Optics.

(g) Detailed conversations have been held with many interested astronomers, including consignment of suitable dissectors to several observatories and space flight centers.

In brief, the smoothing dissector has been shown to be an extremely promising new detector for low light level astronomy and optical detection in space. Perhaps it may even "revolutionize" astronomical detection techniques.

4.0 LOW LEVEL FLUX SOURCE

4.1 PMT Tests

Determination of the absolute counting efficiency of a PMT requires knowledge as to the exact number of emitted photoelectrons at low emission density levels (typically below $1000 \text{ e}^-/\text{cm}^2/\text{sec}$ or below $10^{-16} \text{ A}/\text{cm}^2$). Such levels are generally below those which can be reached with accurately calibrated micro-ammeters.

Alternatively we have attempted to generate a flux source of known intensity at a sufficiently low level to generate the above emission current densities. This could be done in the usual manner, by attenuating a known flux beam of higher (and therefore accurately measureable intensity) to a lower value using nominally neutral filters of known transmission.

Table 4.1 shows a comparison between the measured transmission of a group of 1,2,3,4 and 5 filters, (last row) compared to the expected transmission calculated from attenuation measurements made on the individual filters themselves.

Reasonable care was taken to skew mount the filters, use collimating apertures, and trap all reflected and scattered light. The large difference, almost a factor of 2, between the calculated and measured optical transmissions is indicative of the difficulties which can be encountered using this "brute force" technique.

TABLE 4.1

Measured versus Calculated Filter Transmission

Filter	Measured Transmission (single filter)	Measured Transmission (cascaded filters) (Note 1)	Calculated Transmission (cascaded filters) (Note 1)	Ratio, measured to calculated transmission
1	8.0×10^{-2}	8.0×10^{-2}	8.0×10^{-2}	1.00
2	8.1×10^{-2}	7.08×10^{-3}	6.48×10^{-3}	1.09
3	7.0×10^{-2}	6.56×10^{-4}	5.05×10^{-4}	1.30
4	7.0×10^{-2}	5.41×10^{-5}	3.54×10^{-5}	1.53
5	7.55×10^{-2}	5.18×10^{-6}	2.67×10^{-6}	1.94

Note 1: For cascaded filter combinations up to and including the filter listed.

4.2 Smoothing Dissector Tests

Our tests on smoothing dissectors were made using a different method of attenuation. The emission current from the photocathode under test is measured with a calibrated micro-micro-ammeter using a known (0.712 cm^2) optical defining aperture inserted in a flux beam of uniform intensity (see Section 7.0 and 8.0 below). The cathode current density in amperes/ cm^2 could then be calculated (current density = measured current/.712).

Attenuation of this rather large current (10^{-12} - 10^{-13} A/cm^2) down to levels suitable for low light level and counting tests was then accomplished by the use of an image dissector with a small aperture (25μ diameter). Thus the current entering the aperture was reduced by the ratio (π) $(25 \times 10^{-4})^2/4 = 4.9 \times 10^{-6}$. This was sufficient attenuation to reach the necessary low test levels.

It was assumed that the electron-optical magnification for both the image tube(s) and the Vidisector[®] tube was unity. Corrections for departures from unity could be made if desired, perhaps by measuring the above ratio at high flux levels.

Some possible error due to nonuniformity of the emission current density could also be present.

This project did not procede far enough to permit quantitative measurements of the absolute counting efficiency or absolute S/N ratio of smoothing dissectors to be made (see below)

[®] Registered Trademark, International Telephone and Telegraph Corporation.

5.0 THEORY OF SMOOTHING

It is possible to describe the basic principles behind the smoothing dissector principle in various ways, for example:

(a) in terms of detection of the discrete, bright light flashes produced at the phosphor screen of an image intensifier tube which persist long enough to allow for detection when raster scanning over an image area.

(b) in terms of information "storage" in the phosphor screen, knowing that "storage" is a well-known method of improving camera tube performance.

(c) in terms of a separation of the "noise-bandwidth" of a system (which sets the S/N ratio) from the external circuit bandwidth (which sets the rate at which image elements can be interrogated).

(d) in terms of a time dispersion of quantum events, increasing the "odds" of detection during scan.

Each of these methods of description will lead to equivalent analytical results, since they describe the same basic physical configuration, but each has its own advantages and disadvantages as regards clarity of understanding for individual investigators.

Our initial analytical efforts (Refs 6,7) were largely centered around (d), the description in terms of the dispersion of quantum events to increase the odds of detection.

More recently, we have expanded on this earlier procedure and have published an IIT Technical Note (No. 115) entitled "The Smoothing Dissector, a novel means of Image Scanning", dated July, 1970. This note appears in appendix B.

In summary this note shows that:

(a) a smoothing dissector generating "G" photoelectrons at the dissector photocathode for each photoelectron from the first photocathode of the image intensifier tube, can be expected, under the correct scan conditions, to have an electron counting efficiency and an S/N current ratio, improved by the factor $(G)^{1/2}$.

(b) to achieve the full improvement factor, $(G)^{1/2}$, it is necessary that the sampling time, Δt , per image element (the time to move over one image element) satisfy the "fast sampling" condition

$$\text{Condition 1} \quad \Delta t \leq \tau / G \quad (\text{the "fast sampling" condition})$$

where τ is the combined decay time of the phosphor screen(s) involved.

(c) for the special case where n resolution elements are to be scanned, and a counting efficiency (or S/N ratio) approaching n individual photomultiplier tubes is to be achieved (i.e. the perfect scanning detector) then two additional restrictions must be met:

$$\text{Condition 2} \quad G \geq n \quad (\text{the "high gain" condition})$$

$$\text{and Condition 3} \quad n \Delta t \leq \tau \quad (\text{the "fast repetition rate" condition})$$

Conditions 1, 2 and 3 are the three predicted smoothing conditions to be met, if the full advantages of smoothing are to be achieved. A goal of our experimental program (only partially achieved) was to check the validity of these three basic conditions.

6.0 FREQUENCY RESPONSE

Measurements were made of the frequency response of a one and a two stage smoothing dissector made by fiber optic coupling either one or two stage of "Generation I" F4700 25 mm image intensifier tubes directly to an F4011 fiber optics input Vidisector tube. A Monsanto MV50 Light Emitting Diode (LED) was used as the (650 nm) light source, and a Princeton Applied Research Model 121 synchronous Lock-In Amplifier used to simultaneously modulate the LED and detect the resultant output signal current modulation from the image dissector tube. This synchronous detection technique was selected in order to operate at the lowest light levels possible without going into a single electron counting mode of operation.

The basic test configuration is shown in Figure 6.1.

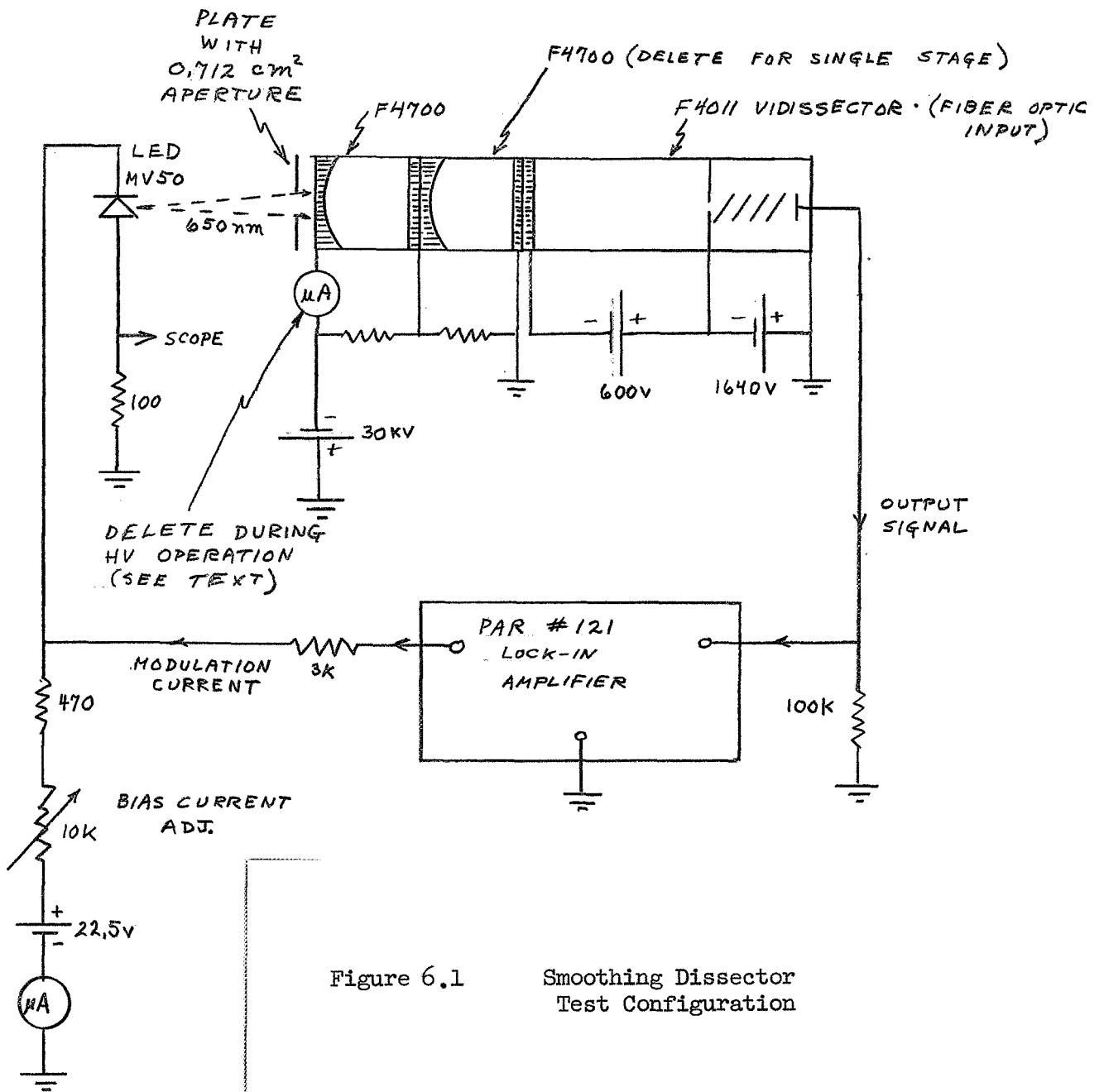


Figure 6.1 Smoothing Dissector Test Configuration

An area of 0.712 cm^2 on the input photocathode was flooded with the 650 nm radiation. Total DC emission current I_k in amperes from this photocathode area was measured prior to application of the high voltage and the LED modulation, using a separate 300 volt current-collecting power supply, thus yielding a known cathode current density, J_k , in A/cm^2 given by $I_k/0.712$. The phosphor bombarding current density was approximately equal to J_k , since the F4700 tubes have nominally unity electron optical magnification.

Modulation current was then applied to the LED, and an AC output voltage signal from the F4011 developed across a 100K load resistor. Modulation frequency on the LED was adjusted with the frequency setting on the lock-in amplifier from 5 HZ to 20 KHZ. All response data was normalized to the 5 HZ value. In general, integration times between 0.1 and 0.3 seconds were selected for the synchronous detector meter circuit. Occasionally, times as long as 3 seconds were needed to avoid excessive meter fluctuation.

Response versus modulation frequency (the amplitude transfer function) was measured for the one stage tube for 3 different excitation current density levels and several peak-to-peak modulation amplitudes of the existing LED flux source (10, 16, and 30%). For the two stage combination, data were taken only for one excitation current density ($1.1 \times 10^{-10} \text{ A/cm}^2$) and input modulation (10%). The results are shown in Figure 6.2.

A correction for the finite bandwidth (69 KHZ) of the measuring meter circuit was made according to

$$\text{Corrected relative response} = \frac{\text{measured relative response}}{\left[\frac{1}{1 + (f/69000)^2} \right]^{1/2}}$$

The F4011 was focussed (giving a 25 micron round sampling area) but (for these measurements) not scanned, since scanning would introduce spurious signals

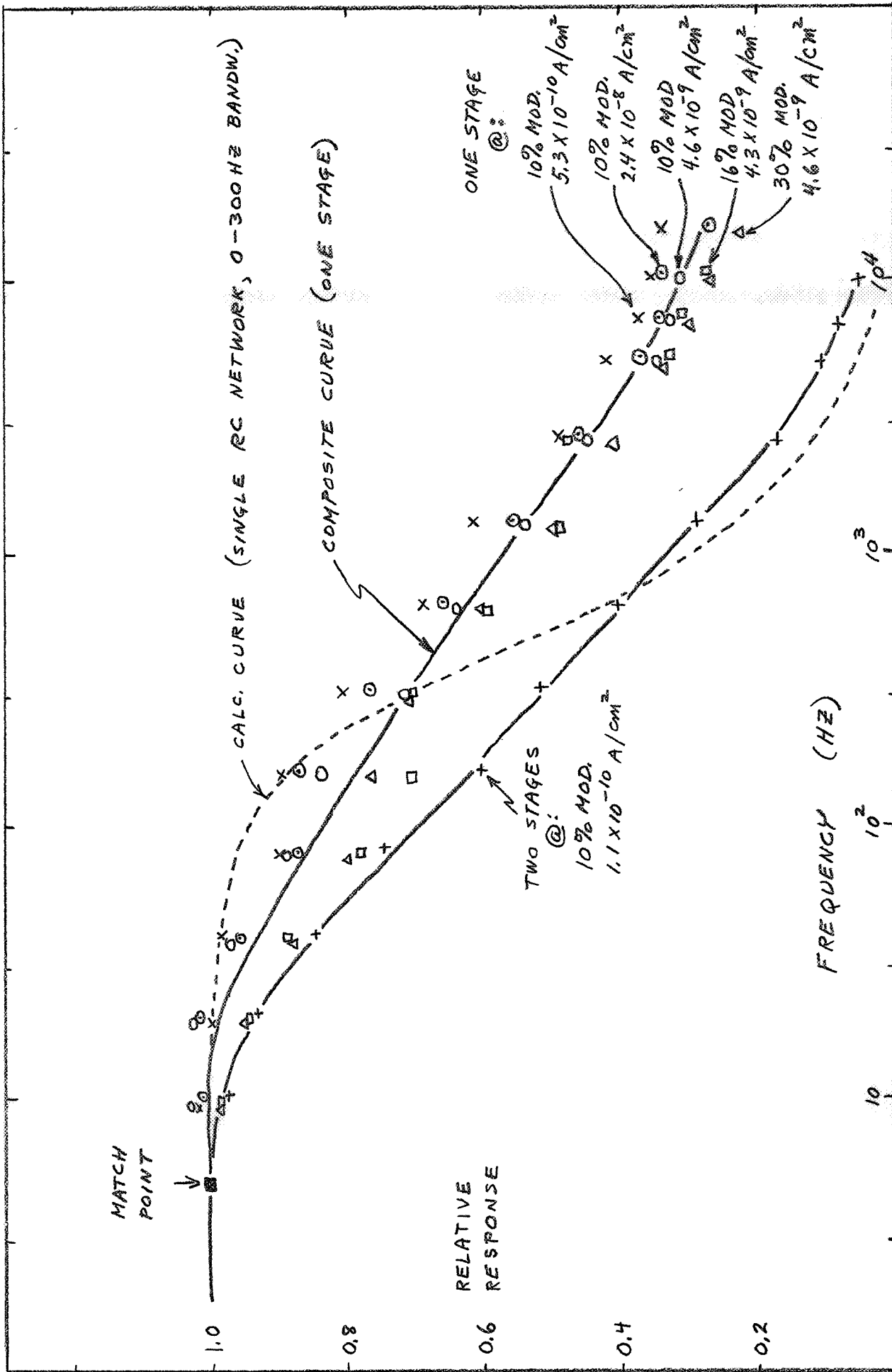


Figure 6.2 Response Time Characteristics of Smoothing Dissectors

due to area response non-uniformities. Possible minor defocussing of the image tubes by the magnetic focussing field of the Vidisector (about 20 gauss) was ignored.

6.1 Interpretation of the Results

No significant differences in the amplitude transfer function were observed at the different current densities and percentage modulations selected for the single stage tube (see Figure 6.2) although there does appear to be some increase in response speed with increased excitation current. It is possible that differences would have been seen if a wider range of excitation levels had been selected, especially if the excitation were increased to the point where the phosphor screen are normally used for CRT displays. The test data observed here under low excitation conditions should be applicable to many low level applications of smoothing dissectors.

The 70.7% amplitude response point (3 db power point) for the single stage tube occurs at approximately 300 HZ. This is reasonably consistent with the expected behavior of P20 type phosphor screens (as used in the Fl4700 tubes) and with the integral response data of McNall, Robinson and Wampler (Ref. 1), who observed a time of approximately 100 μ sec for 50% of the photon output from a similar single stage (Generation I) tube under single electron excitation conditions.

For the two stage combination (also shown in Figure 6.2) the observed behavior, at 1.1×10^{-10} A/cm² and 10% modulation, was 70.7% transfer response at approximately 90 HZ (the 3db point), i.e. substantially slower than a single stage tube. This is consistent with the expected behavior for two cascaded phosphor screens (the 50% response) for the two stage tube being approximately 370 HZ).

The dotted curve in Figure 6.2, shows the calculated behavior of a simple exponential ("RC") type decay. It can be seen that the P20 phosphor screens (as expected) do not approximate a simple exponential law decay. Perhaps a double exponential decay or even a hyperbolic decay would more accurately describe their behavior.

It should be emphasized that data of this type is not readily available in the technical literature. Most of the reported phosphor screen response time data pertains to higher excitation levels, as used in CRT applications, and cannot be applied here, with reliability, to the performance of threshold devices, such as the smoothing dissector.

7.0 LINEARITY

The response linearity (DC output current vs DC flux input) of a one and a two stage smoothing dissector was checked as follows:

The basic test configuration is the same as the one shown in Figure 6.1, but with the following modifications: the synchronous amplifier was removed so that unmodulated flux from the LED excited the input photocathode. The DC output current from the anode of the F4011 Vidisector was measured with a calibrated Keithley 600B Micro-ammeter, and (with the high voltage temporarily reduced) the DC cathode current from the first photocathode of the image intensifier tube was also measured.

In addition, an FW130 photomultiplier tube, in a circuit previously checked for linear response (output current versus input flux) was used with a Keithley Model 414 microammeter to monitor the relative magnitude of the flux from the LED. This tube looked at a portion of the light emitted by the LED simultaneously with the smoothing dissector under test.

The results of these tests are shown in Figures 7.1 and 7.2. The observed dissector anode current, I_A , and the observed image tube photocathode current I_k , are plotted versus the PMT anode current, I_{PMT} . Figure 7.1 gives the single stage results and Figure 7.2 the double stage results.

For the two stage tests the flux load was decreased, by decreasing the LED bias current, to give approximately the same dissector output current range. The corresponding current from the PMT was also adjusted to about the same range, by increasing the PMT voltage from 1 KV (single stage tests) to 1.2 KV (double stage tests).

As can be seen, the plots of image tube cathode current I_k versus PMT anode current, I_{PMT} , (dashed curves) are essentially exactly linear, indicating a proper test configuration. This check allows us to use the PMT current, I_{PMT} , as an abscissa scale directly proportional to the magnitude of the incident flux, as

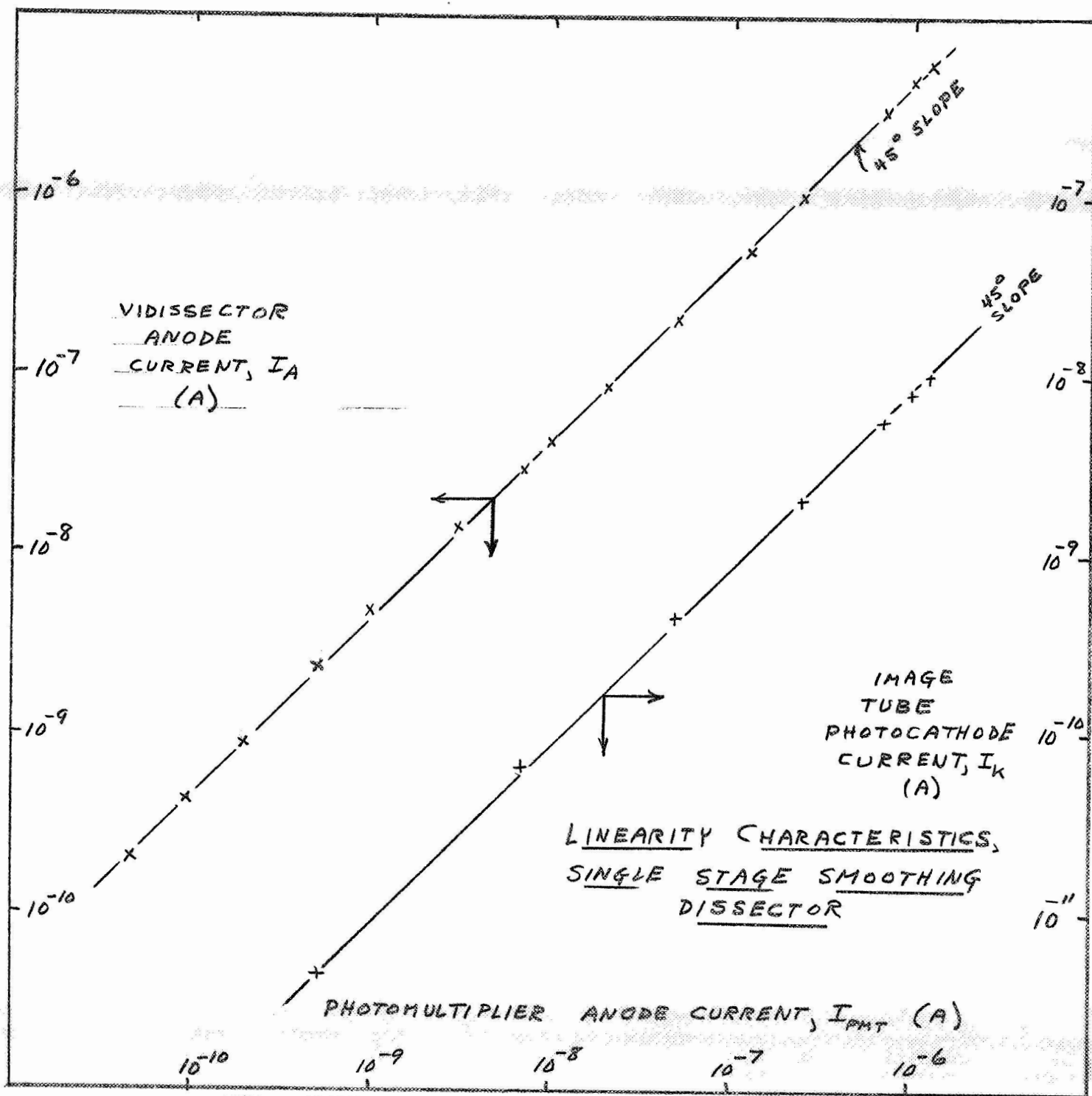


Figure 7.1 Linearity Characteristics, Single Stage Smoothing Dissector

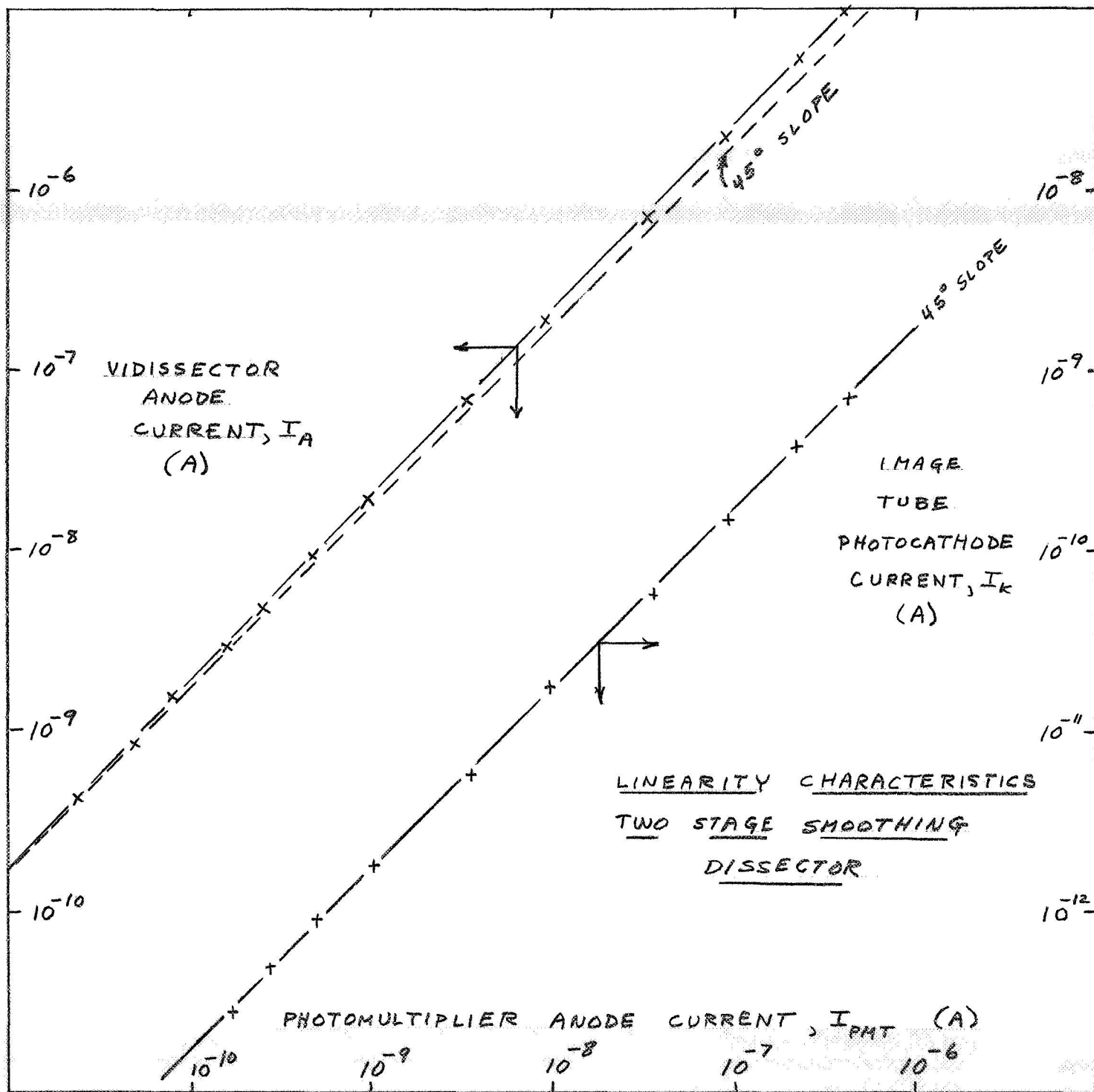


Figure 7.2 Linearity Characteristics
Two-Stage Smoothing Dissector

desired, and extends the working range below the flux level permitted by use of the I_k measurement alone.

For the single stage configuration, Figure 7.1, the observed data (solid curve) on the dissector output current versus relative flux input (I_{PMT}) was essentially linear over the full range tested (approximately 5×10^{-13} A/cm² to 10^{-8} A/cm² for the input photocathode current density).

For the two stage configuration, Figure 7.2, however, the corresponding data indicates a small, but measureable departure from linearity, the 2-stage smoothing dissector appearing to give somewhat super-linear behavior (a slope exceeding the linear 45° dashed line in Figure 7.2).

Several similar repeat measurements were made to confirm this behavior, with the same results. Whether or not this small superlinear behavior is a valid characteristic is not presently known.

8.0 S/N RATIO

Direct measurements were made of the S/N ratio of (1) a Vidisector alone (no smoothing), (2) a single stage smoothing dissector, and (3) a two stage smoothing dissector.

The basic test configuration is the same as the one shown in Figure 6.1. Modulation on the LED light source was removed and the circuit shown in Figure 8.1 was used to directly measure the DC magnitude and the rms magnitude of the output signal current (current due to the flux input) dissector anode.

Since the smoothing dissector is known to have an important dependence on the sampling rates selected for interrogating successive image elements during scan (with a rather complex interrelation with phosphor decay time), measurements of the S/N ratio over a wide range of circuit bandwidths were made, by selecting various combinations of the R and C values in Figure 8.1. Table 8.2 shows the selected

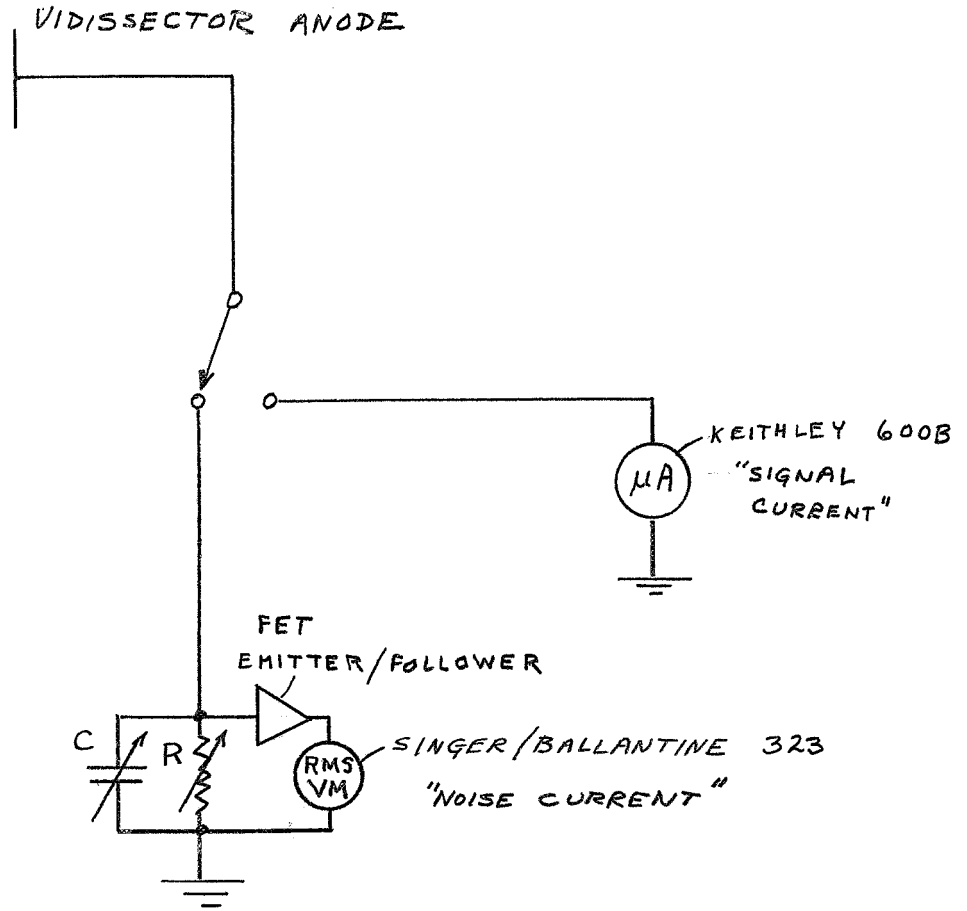


Figure 8.1 S/N Anode Test Circuit

TABLE 8.2

CALCULATED CIRCUIT BANDWIDTH, B (Hz)

External Load Resistor (ohms)	Effective Circuit Resistance (ohms)	Effective Circuit Capacitance (pf)				
		23(note 1)	372	4670	7070	32300
∞	10.216 M	775	42	3.3	2.2	0.48
2.313 M	1.886 M	3.67 K	227	18.1	11.9	2.62
1.015 M	0.922 M	7.5 K	465	37.0	24.4	5.35
0.5292M	512 K	13.5 K	836	66.7	44.0	9.65
0.201 M	197 K	35.1 K	2.17 K	173	114	25
101 K	100 K	69 K	4.28 K	341	225	49.4
51.25 K	51 K	135 K	8.40 K	669	442	96.5
20.56 K	20.5 K	3.38 K	20.9 K	1.66 K	1095	240
10.9 K	10.1 K	685 K	42.4 K	3.38 K	2.23 K	488
5.01 K	5.01 K	1.38 M	85.5 K	6.80 K	4.5 K	985
1.963 K	1.96 K	3.53 M	218 K	17.4 K	11.5 K	2.52 K
990.8	991	6.98 M	432 K	34.4 K	22.7 K	4.97 K
516.2	512	13.5 M	830 K	-	-	-

Note 1: No external capacitance, no "T" connector

computed magnitude of the external circuit 3 db bandwidth (1/2 power bandwidth) B in Hz, for various RC combinations. The noise bandwidth, Δf , in Hz for these simple RC networks is related to the 3 db bandwidth, B, by:

$$\Delta f = (\pi/2) B \approx 1.57 B$$

The circuit bandwidth is linearly proportional to the various sampling rates which could be used with the smoothing dissector to interrogate a series of image elements. Thus, for example, a 1 KHZ 3 db circuit bandwidth would allow for sampling approximately 2 image elements in 1 millisecond, or a sample time of about 0.5 milliseconds. Thus:

$$\text{Permissible sampling time} = \frac{1}{2B} \approx \frac{\pi}{4 \Delta f}$$

No scan and no image sampling (per se) were used in these S/N tests since scanning with a uniformly flooded input only introduces a possible spurious frequency component due to response non-uniformities over the sensitive area (shading, granularity, spots, etc.) without changing the magnitude of the shot noise to be measured from the photocurrent itself (assuming a uniformly flooded photocathode).

Figure 8.3 shows the measured S/N ratio (actually the observed signal current to noise current ratio SNCR, corrected for the input flux level as described below), as a function of the various selected external circuit bandwidth values, B, from 0.5 HZ to 13.7 MHZ. At the extreme lower values, the S/N ratio erroneously appears to improve since the noise voltmeter is failing to read correctly, and at the extreme high values the S/N ratio erroneously appears to increase because of the FET preamplifier losses. But in the mid-frequency range, from approximately 10 HZ to 10^6 HZ the data is representative of dissector and smoothing dissector behavior.

As can be seen, the lower curve, for the Vidissector alone, closely obeys a 1/2-power law, as expected based on the simple noise theory of dissectors and PMT's.

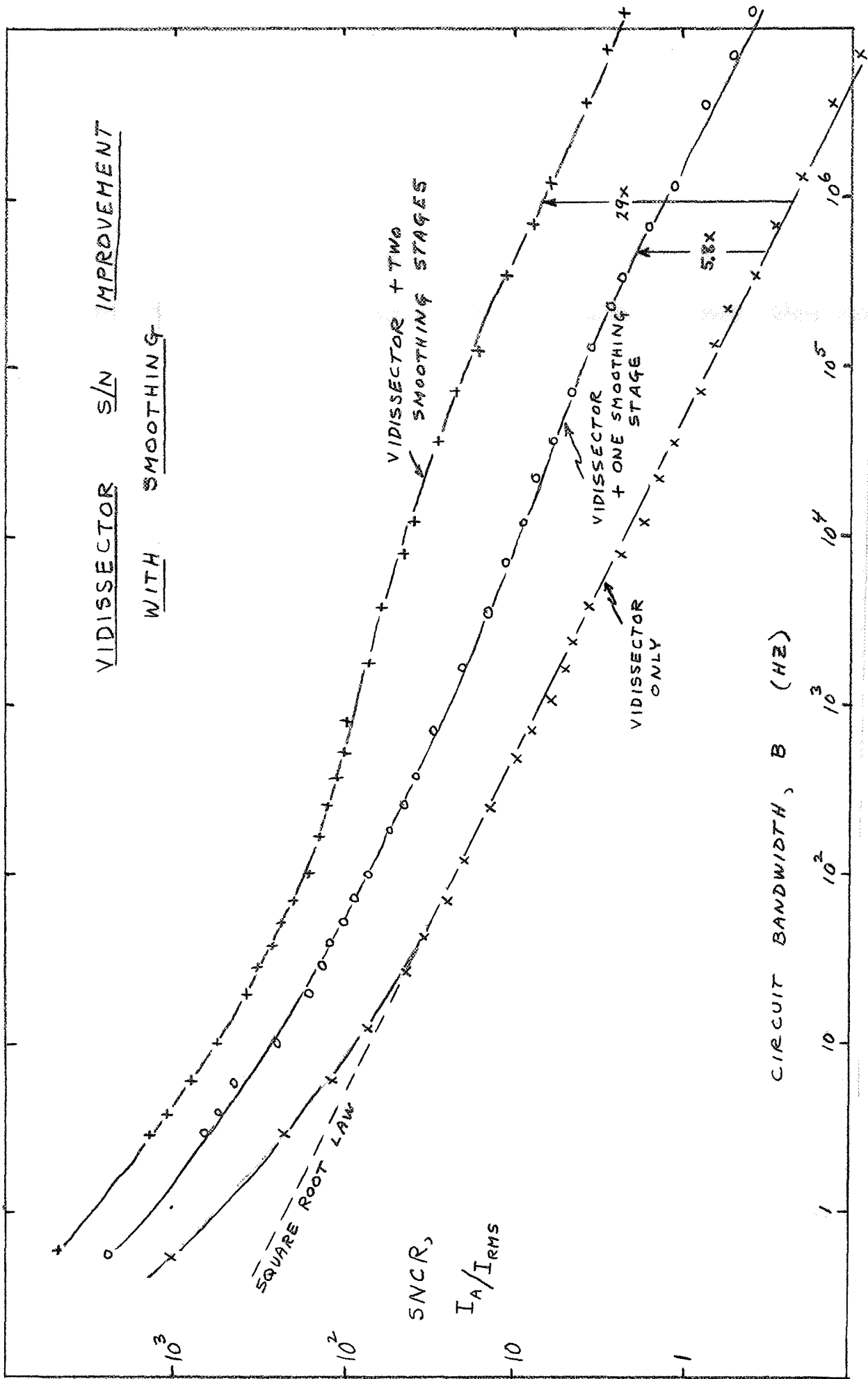


Figure 8.3 Vidisector S/N Improvement with Smoothing

The middle curve, for a single stage smoothing dissector, shows:

(a) an improved magnitude, with smoothing, of about a factor of 5.8 (This agrees with an expected increase according to the theory of smoothing by the square root of the image tube current gain, i.e. $5.8^2 = 34$, compared to the measured current gain of 28)

(b) a tendency to show the best improvement for high frequencies (fast sampling) as expected from smoothing theory.

(c) a corresponding tendency to show less improvement at the lower frequencies (slower sampling rates), again, as expected.

(d) a significant improvement, (about 3 times) even at the lowest frequencies (1-10HZ). This was not an expected result, and will need further interpretation. It may be the result of the broad distribution in the decay characteristics of the phosphor screens (See Section 6.0 above).

Similar behavior was observed for the two stage smoothing dissector, (the upper curve in Figure 8.3), with a gain of about 29 at fast sampling rates (equivalent to a current gain in the two stage intensifier section of about 29^2 or about 850). If S/N power ratios had been plotted in Figure 8.3, the observed improvements would have been linearly proportional to the current gains of the image tubes, i.e. 34 times and 850 times.

The data for Figure 8.3 were taken at a constant current density loading on the F4011 photocathode of 9.05×10^{-9} A/cm². This maintained constant test current conditions in the F4011, but required a readjustment of the test flux (downward) when one and two stage of image intensification were added. For the single stage tube, its measured photocathode loading was

$$3.2 \times 10^{-10} \text{ A/cm}^2$$

which yielded a current gain of $\frac{9.5 \times 10^{-9}}{3.2 \times 10^{-10}} = 28.3$ for this particular F4700/F4011 combination. For the two stage tube the measured input photocathode loading was 1.39×10^{-11} A/cm² giving a net overall gain of $(9.5 \times 10^{-9}) / (1.39 \times 10^{-11}) = 650$.

To show as clearly as possible in Figure 8.3 the effective S/N improvements with smoothing, the measured S/N ratios for the one stage tube were multiplied by

$$\left(\frac{9.05 \times 10^{-9}}{3.2 \times 10^{-10}} \right)^{1/2} = (28.3)^{1/2} = 5.31$$

and the two stage tube by:

$$\left(\frac{9.05 \times 10^{-9}}{1.39 \times 10^{-11}} \right)^{1/2} = (650)^{1/2} = 25.5$$

before plotting. This procedure normalized the three curves in Figure 8.3 to the same equivalent emission current density from the first photocathode (i.e. to the same flux input if the three photocathodes were identical in response), and thus shows more clearly the gains in S/N ratio with smoothing.

Table 8.4 compares the measured current gain, with one and two stages, with the measured improvement in S/N power ratio. The discrepancies seen between theory and experiment (with the measured S/N ratios improved more than the predicted amounts, based on the measured current gains) may well be due to errors in our experimental measurements (which involve low emission current measurements and difficult S/N measurements). In any case the measured S/N power ratio increase exceeded that predicted from elementary smoothing theory.

The magnitude of the S/N power ratio improvements observed (34 and 850 times) should be stressed. These magnitudes may well be sufficient to make the image dissector, with smoothing, competitive with, or even superior to other means of image scanning.

TABLE 8.4

MEASURED CURRENT GAIN VS MEASURED S/N IMPROVEMENT

No. of Stages	Measured Current Gain	(Measured SNCR increase) ²
1	28.3	34
2	650	850

9.0 PERFORMANCE AS A SPECTRUM SCANNER

To check the performance of the smoothing dissector as low light level spectrum scanner (perhaps its most important immediate application) we set up the test configuration shown in Figure 9.1. The F4700 25 mm electrostatic-focus fiber-optic image tube (either one or two stages) was directly coupled by optical butt coupling to the fiber optics input of the F4011 Vidisector.

The sawtooth signal from the monitoring scope sweep was used to drive the magnetic deflection circuit of the F4011, avoiding synchronization problems. Dissector and image tube operating voltages were the same as in earlier tests. (Section 7.0).

The optical test pattern was the demagnified image of a Westinghouse EFT-1332 test chart, shown in Figure 9.2a. This chart simulated an optical spectrum with a line pairs pattern ranging from 2 line pairs/mm to 20 line pairs/mm at the input photocathode. Since the dissector scanning aperture was 25 microns in diameter, its diameter was approximately equal to the width of one white bar of the finest pattern (20 lp/mm), and would have given nearly 100% signal modulation for this line density at high light levels, perfect focus conditions, and wide bandwidth.

A sweep rate of 10 sweep/second (10 ms/cm on the scope face) was selected, giving an aperture sampling time of about 300 μ sec (a time of 300 micro second to move one aperture diameter). To minimize modulation amplitude losses due to finite circuit bandwidth, a circuit bandwidth of 5.75 KHZ was selected for the scope preamplifier.

The test chart was illuminated by a tungsten lamp or LED diode at various (and unspecified) flux levels, but the photocurrent from the first photocathode was monitored, as in Section 6.0, with the test chart removed and a 0.712 cm² aperture added, to determine the photocathode emission current density in the image highlight areas for all tests.

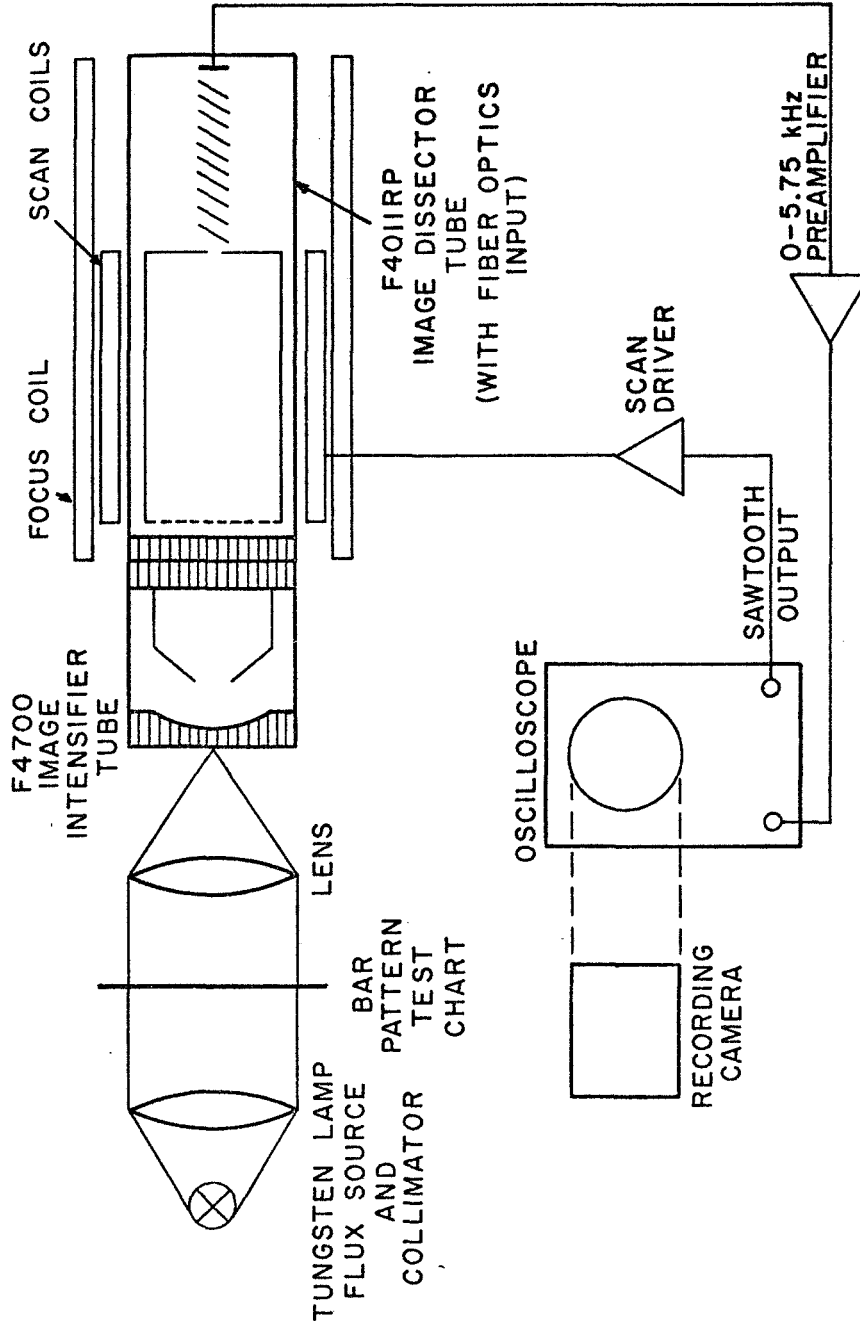


Figure 9.1: Basic Smoothing Dissector Configuration

Figure 9.2

(Figure 9.2 is identical to Figure 2 of Appendix A)

Figures 9.2 b-d shows reproductions of the typical output current signals recorded. (over 300 photographs were taken). Figure 9.2b shows the results, at one flux level (producing 1.8×10^{10} e⁻/cm²/sec) with a one stage smoothing dissector. Figure 9-2c shows the results for a dissector alone (no smoothing) at the same flux level, and Figure 9.2d shows the results for the dissector alone, but at 20 x higher flux level.

Examination of Figure 9.2 fully confirms the expected improved capability of the smoothing. The signal-to-noise ratio, and the resulting ability to detect the line pairs pattern, is as good as the dissector alone can do at 20 x higher flux level. Thus the smoothing dissector can extract as much information as 20 separate dissectors or 20 separate scanning photomultiplier tubes.

This is a noteworthy achievement, and one which may indeed "revolutionize" certain aspects of astronomical detection.

Table 9.3 summarizes the test results for one and two stage smoothing dissectors. This table shows the measured emission current levels at which the ability of the device to detect the optical spectrum in these two configurations equal that of the dissector alone, and the resultant improvement ratios.

As can be seen, this particular one stage dissector seems to be consistently 20-25 times better than a dissector alone, while a two stage tube runs from 40-100 times better.

It should be noted that the amplitude modulation ratios obtained with the one and two stages added, were inferior to that obtained with the dissector alone, even at high flux levels, where noise did not interfere with the measurement. The measured results are shown in Table 9.4. Undoubtedly this loss of "resolution" was partly due to the limited resolving power of the image tubes, enhanced by the defocussing effects on these tubes by the weak magnetic focus field of the Vidisector. No attempt was made here to optimize focussing by use of a fiber optic boule coupler to help isolate the image tubes from this magnetic field.

TABLE 9.3

PATTERN DENSITY FOR VARIOUS DISSECTOR CONFIGURATIONS

Line Pairs/mm at 50% Modulation		
Dissector only	Dissector plus one smoothing stage	Dissector plus two smoothing stages
16	10	6

TABLE 9.4

EQUIVALENT PHOTOEMISSION LEVELS

Dissector only (A/cm ²)	Dissector plus one smoothing stage (A/cm ²)	Dissector plus two smoothing stages (A/cm ²)	Improvement Factor with smoothing	
			one Stage	two stages
2×10^{-11}	1×10^{-12}	5×10^{-13}	20	40
2×10^{-10}	1×10^{-11}	5×10^{-12}	20	40
1×10^{-9}	5×10^{-11}	2×10^{-11}	20	40
5×10^{-9}	2×10^{-10}	5×10^{-11}	25	100
2×10^{-8}	1×10^{-9}	2×10^{-10}	20	100

9.1 Single Electron Counting Characteristics

At the lowest flux levels used in the spectrum scanning, the output signal current breaks up, as it does in photomultiplier tubes, into discrete, easily counted pulses. While we had no counting equipment with the necessary time-to-height convertor for displaying a spectrum on a multi-channel analyzer, we could count the pulses obtained photographically at various light levels.

Figure 9.5 shows the results (hand traced off the original photographs) of the pulses obtained at several low flux levels, with the dissector alone and with one and two stages of smoothing.

The distinct improvement in the absolute photoelectron counting efficiency (and thus of the detective quantum efficiency) in the smoothing process is clearly shown.

The sweep times in Figure 9.5 were only 20 milliseconds, since the 5 x magnifying sweep was being used in these photos. At 7×10^{-13} A/cm², neither the dissector alone, nor the single stage unit, happened to observe a single photoelectron whereas the 2 stage tube detected 3 events. At 7×10^{-12} A/cm² the dissector alone still observed nothing, but the single stage tube now detected about 11 electrons, and the 2 stage tube detected over 35 electrons, etc.

It is quite clear, from the results recorded in Figure 9.5 and in the additional photographic results, that the photoelectron counting efficiency is markedly improved by smoothing, and, by about the ratio predicted by the elementary theory of smoothing. (Refs. 3,4,5,6,7)

A repetition rate of 10 sweeps/second was selected for all of our recorded simulated optical spectrum scan tests. This rate was probably somewhat slow if 100% photoelectron counting efficiency were to be a desired goal, since most of

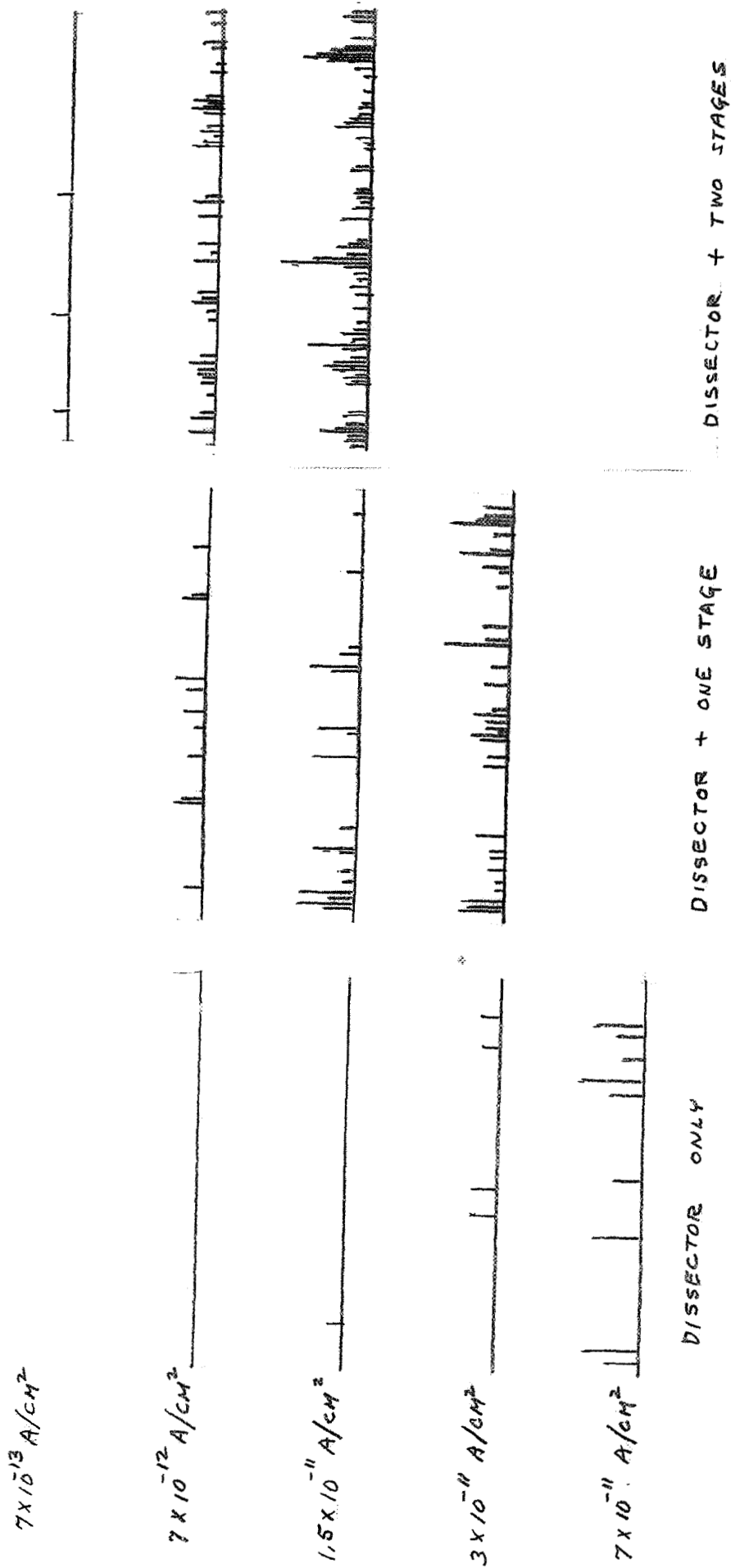


Figure 9.5 PULSE COUNTING CHARACTERISTICS OF A SMOOTHING DISSECTOR

photons from a single electron event occurring just after a scan interrogation would be decayed in the 0.1 second time interval before the next interrogation. Furthermore, the sampling time of 300 μ sec, while probably short enough to avoid appreciable multiple sampling of single electron pulses (a primary smoothing requirement) might well have been shorter yet.

Perhaps faster sweep rates, and shorter sampling times would have helped make the gain obtained with two stages of smoothing (only about 40-100) approach more nearly the expected improvement of $(20)^2 = 400$ (compare Table 9.3 and the Section 8.0 results).

Despite these somewhat restrictive choices on time constants the observed gain in S/N ratio with smoothing was substantial.

Further tests, under different repetition rates and sampling times are clearly desirable.

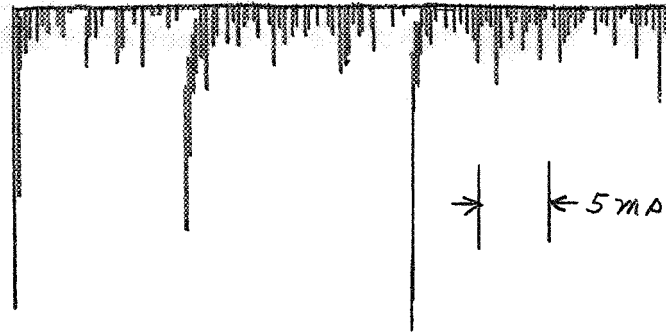
A summary of the results reported here, and reprinted as Appendix A, has been accepted by Applied Optics for publication, and is due to appear in the August 1971 issue.

9.2 SINGLE ELECTRON SCINTILLATIONS

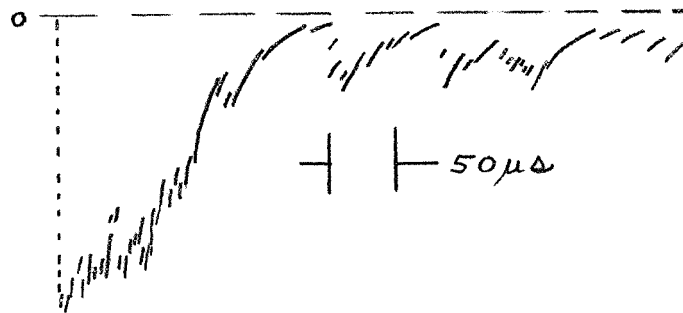
The single electron scintillation properties of a two stage smoothing dissector were investigated by stopping the scan, and looking at the output signal pulses from the dissector anode with an oscilloscope at a very low light level (1.3×10^{-12} A/cm² at the first photocathode or 40 electrons/second through the 25 micron aperture).

Figure 9.6 a shows a tracing of a typical signal at 5 ms/cm (50 ms/sweep). The three large pulses were probably scintillations due to photoelectrons from the first photocathode (2 were expected, on the average, for this sweep rate). The background of smaller pulses were presumed to be due to delayed photon emission from the two phosphor screens (from earlier scintillations) as well as from thermionic emission from the second and third photocathodes and the electron multiplier. Some evidence of intermediate-sized pulses, perhaps due to scintillations at the second phosphor screen can be seen in the original photographs. The time constant to the 50% point for the larger scintillations seems to be about 1 ms, which is reasonably consistent with the measured behavior of two stage tubes (Section 6.0).

The larger scintillation pulses were observed in more detail, by triggering the scope sweep only for large pulses and increasing the sweep speed to 50 μ sec/cm or 0.5 ms/sweep. A typical result is shown in Figure 9.6b, traced off the original photograph. The discontinuities in this sweep (which have rise times of about 10-20 ns, and therefore appear as discontinuities at this sweep speed) can be attributed to single electron events at the dissector aperture. Thus, each scintillation appears to be composed of about 50-100 single electron pulses in the dissector multiplier, down to about 10% pulse amplitude. This occurs in 0.5 milliseconds, which is again consistent with other measurements of two stage decay time behavior.



(a) SLOW SCAN



(b) FAST SCAN

Figure 9.6

OUTPUT PULSES FROM TWO
STAGE SMOOTHING DISSECTOR

It should be noted that this direct observation of output scintillations could not be used to measure the absolute photon counting efficiency of a two stage image intensifier tube.

10.0 ABSOLUTE SPECTRAL RESPONSES

Figure 10.1 shows the measured absolute spectral response of the three detectors used. Since the F4011 Vidisector had a conventional (S20) multi-alkali photocathode, while the two F4700 single stage image intensifier tubes had extended red response, no attempt was made to put equal flux levels onto the different tube combinations. Instead, for each experiment, the total photocurrent emitted from the first photocathode was measured with a sensitive micro-ammeter, with a 0.712 cm² round defining aperture in front of the photocathode.

The emission current density J_k (which is the factor controlling the detector performance following the photocathode) could then be calculated from:

$$J_k \text{ (A/cm}^2\text{)} = \frac{I_k \text{ (measured cathode current in A)}}{0.712}$$

To make this measurement, only enough voltage (approximately 300 volts) was applied to assure that all photocurrent was collected. For further details, see Sections 6.0 and 7.0.

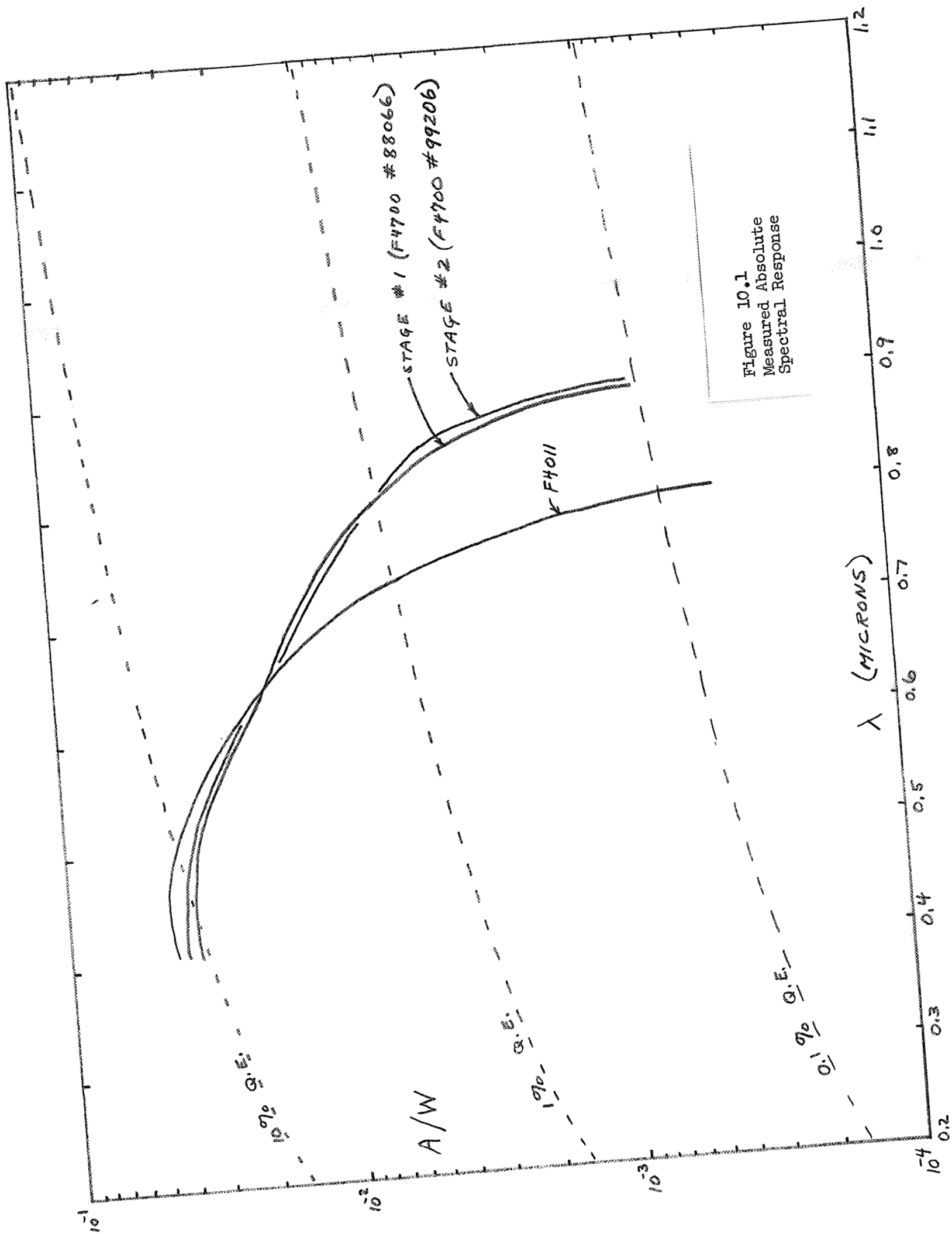


Figure 10.1
Measured Absolute
Spectral Response

11.0 TECHNICAL MEETINGS

During the period of this contract several key meetings were held with interested astronomers and space scientists. These included Dr. Kenneth Hallam, Charles Aitken, Gerald Baker, Dr. James Kupperian, Mr. William White, Edward Chin and Larry Dunkelmann of Goddard Space Flight Center, James Milligan of Marshall Space Flight Center, Dr. E. J. Wampler of Lick Observatory, Dr. E. Dennison and Dr. J. B. Oke of Mount Palomar Observatory, Dr. Robert Tull of McDonald Observatory, Dr. Roger Lynds of Kitt Peak Observatory, Dr. A. Hiltner, President of AURA, Dr. Kent Ford and Lewis Brown of the Carnegie Institution.

ITTT is attempting to maintain close liaison with as many working astronomers as possible to help keep them abreast of the work being done on this contract, and the potential advantages of quantum counting photomultipliers and dissectors.

12.0 GENERAL CONCLUSIONS

During the period of this contract, the potential advantages of the smoothing dissector technique for astronomical readout have been more fully confirmed. While a number of un-answered questions remain, it is clear that use of image intensifier tube (or tubes) ahead of an image dissector does offer many advantages over other techniques for certain applications.

In particular the use of a dissector with a slit aperture, scanning a low light level spectrum, in the quantum counting mode, may be an especially valuable technique. Present procedures either use photographic recording (low quantum efficiency and delayed readout), electronography (technologically difficult), or TV type readout (low resolution, non-quantum counting). Each of these alternative techniques suffers from one or more serious disadvantages.

13.0 REFERENCES

1. J. McNall, L. Robinson, E. J. Wampler, Publ. Astr. Soc. Pac 82, 837 (1970)
2. W. K. Ford, Jr., and L. Brown, Carnegie Institution Year Book 69, 370 (1971).
3. K. J. Hecker, M. P. Nordseth, H. M. Joseph U S Patent 3,355,616 (1965)
4. M. Namoridi, Analysis of the Image Dissection Image Tube, Document AD-639-067 (1966)
5. W. L. Wilcock, S/N Ratio Analysis for Dissection Tube, (Private Communication)
6. E. H. Eberhardt, IIT Research Memo 398, Smoothing Electron Multipliers (1964)
7. G. Papp, IIT Research 403, Smoothing Multiplier Principle as Applied to an Intensifier Image Dissector; (1964).

APPENDIX A

A Method of Improving the S/N Ratio of an Image
Dissector for use in an Electronic Scanning
Spectrometer

(This appendix contains a copy of a publication prepared for and accepted for
publication in Applied Optics, August, 1971)

ELECTRON TUBE DIVISION
Tube and Sensor Laboratories
3700 East Pontiac Street
Fort Wayne, Indiana 46803
Telephone 219 743-7571

APPLICATIONS NOTE E17

**A METHOD OF IMPROVING THE SIGNAL-TO-NOISE RATIO
OF AN IMAGE DISSECTOR FOR USE IN
AN ELECTRONIC SCANNING SPECTROMETER**

Hecker, Nordseth and Joseph have suggested (Ref. 1) a novel means of extracting information from an optical image, using an image dissector which has been internally modified by the addition of a method of image intensification followed by a slow decay phosphor screen prior to the dissecting aperture. In this modified image dissector the slow phosphor screen acts as a temporary storage element, offering the possibility of an improved signal-to-noise ratio.

McNall, Robinson and Wampler, using an ITT FW130 photomultiplier tube in the single electron counting mode, have experimentally investigated (Ref. 2) the time dispersion and related statistical properties of one, two, and three stage electrostatically focussed image intensifier tubes when excited by single input quanta. They show that these properties are indeed appropriate for improving the information extraction from optical images (increasing the detective quantum efficiency), especially from low light level spectra, if such image intensifier tubes were to be used in conjunction with line scanning image dissectors. Further experimental confirmation has been reported by Ford and Brown (Ref. 3) who have coupled an image dissector (an ITT F4011) to a two stage high gain magnetically focussed image intensifier tube, and shown that the short time (approximately 1 millisecond) storage of the image tube is sufficient to permit counting of the primary photoelectron scintillations in the line scan mode.

We have now shown that the combination of an image intensifier tube coupled to the input of an image dissector, which we call a "smoothing dissector", can also be used to advantage at higher light levels in a more conventional current-measuring (non-quantum-counting) mode. In our technique we observe the output current from the smoothing dissector anode directly on an oscilloscope or other similar recording instrument.

Our basic test configuration is shown in Figure 1. A single stage electrostatically-focussed ITT F4700 image intensifier tube, with an S25 type input photocathode and a P20 type output phosphor screen, is fiber-optically coupled to an ITT F4011RP image dissector tube, with an S25 type photocathode and a 25 micron diameter dissecting aperture. The output current from the F4011RP is fed through a conventional preamplifier, having a DC to 5.75 kHz half power bandwidth, to a Tektronix Model 543/1A1 oscilloscope.

ELECTRON TUBE DIVISION 

To demonstrate the special detection capability of this smoothing dissector as a spectroscopic detector, and to simultaneously display the spacial modulation properties, we simulated a low light level input spectrum with the image of a portion of a Westinghouse ET-1332 bar pattern test chart, Figure 2a, reduced in size to give ten sets of repetitive bars ranging in repetition density in steps of 2 line pairs/mm from approximately 2 line pairs/mm to 20 line pairs/mm at the input photocathode. This optical test image was then line-scanned with the smoothing dissector at 100 ms/sweep, using the sawtooth output from the oscilloscope for horizontal deflection.

Figure 2b shows the output signal current observed on the oscilloscope for an input flux level yielding a measured current density of 1.8×10^{10} electrons \cdot cm⁻² \cdot sec⁻¹ in the image highlight areas from the photocathode of the F4700. This image intensifier tube was operated at approximately 15 kV overall, at which voltage each photoelectron striking the phosphor screen typically triggers the emission of about 500-1000 photons exiting from the output fiber optics window.

For direct comparison, Figure 2c shows the signal output current obtained under the same conditions, but with the image intensifier tube removed, and the input image focussed directly onto the photocathode of the image dissector. In this case the input flux level was slightly readjusted, to compensate for the small spectral response differences between the two photocathodes, to give the same measured highlight emission current density (1.8×10^{10} electrons \cdot cm⁻² \cdot sec⁻¹) from the photocathode of the image dissector. The ability of the smoothing dissector to improve the signal-to-noise ratio, i.e. to increase the overall detective quantum efficiency of this scanning detector, is clearly evident when comparing the results shown in Figure 2c with those shown in Figure 2b.

To determine the approximate amount of improvement obtained, we then increased the flux level incident on the dissector alone by a factor of 20 (to 3.6×10^{11} electrons \cdot cm⁻² \cdot sec⁻¹) and recorded the resulting scan signal, Figure 2d. Comparison of Figure 2d with Figure 2b shows that our particular F4700/F4011RP smoothing dissector combination had an information extraction capability equivalent to an increase of approximately 20 times in the flux level, or to the use of approximately 20 separate photomultiplier tubes, each scanning 1/20 of the optical spectrum. Further improvement should be possible by the use of additional stages of image intensification ahead of the image dissector.

While a definitive theory of smoothing has not yet been published, our own analysis indicates that our test configuration meets the basic requirement for smoothing, namely, that the same time for each resolvable image element (approximately 0.1 ms in our case) be shorter than the phosphor decay time (about 0.5 ms for the F4700).

As shown in Figure 3, we have also confirmed the input/output linearity of our smoothing dissector using a Monsanto MV-50 GaAs light emitting diode, whose 650 nm output flux could be conveniently varied over a wide dynamic range by changing the applied excitation current. The relative output flux from this diode was monitored with an ITT FW130 photomultiplier tube. The actual magnitude of the flux density incident on the image intensifier tube at the higher irradiance levels was then determined by measuring the F4700 photocathode emission current, using a 0.712 cm² round optical defining aperture and the measured radiant sensitivity of the F4700 photocathode at 650 nm (18 mA/W). The relative flux density readings, taken with the photomultiplier tube over the full range of irradiance levels, were then matched

to these absolute values. No evidence of non-linearity was observed, even at the lowest flux levels, where single electron excitation events could easily be observed on the oscilloscope, and where Francis and Stoudenheimer (Ref. 4) have reported non-linear behavior of P11-type phosphor screens.

It seems reasonably clear from our results, and from those of McNall, Robinson and Wampler, and Ford and Brown, that the smoothing dissector offers the following advantages over other techniques for spectroscopic detection:

1. It has a higher detective quantum efficiency, i.e. a higher information extraction capability, and thus a better signal-to-noise ratio than either a single scanned photomultiplier tube or a scanning image dissector.
2. It is less complex and probably less costly than an equivalent array of photomultiplier tubes.
3. It can be used either in the digital (quantum-counting) mode of operation at very low light levels, or, in the analog (current-monitoring) mode of operation at higher light levels.
4. It can be single line scanned, using a slit-shaped aperture matching the desired spectral resolution, instead of inefficiently raster scanned as in conventional storage-type television camera tubes.
5. The scan can be localized, upon command, to examine selected spectral regions in more detail and with a higher signal-to-noise ratio.
6. The scan can be stopped completely on any desired single spectral element, and the smoothing dissector then used as a single premium photomultiplier tube.
7. The output information, whether analog or digital, is quantitative in nature, and linearly proportional to the input flux density over several orders of magnitude.
8. The output information is immediately available, not time-delayed as in conventional photography, for transmission to remote monitoring stations, where possible feedback control can be exercised (optical focussing, electrical focussing, selection of localized scan areas, etc.).
9. The input image intensifier tube can be electrically gated for use in time-resolved spectroscopy.
10. The spectral information from very short optical pulses is temporarily stored in the phosphor screen(s) for subsequent scan readout.
11. The spectral response can range from approximately 110 nm in the UV to 1200 nm in the IR.

In addition, because of the inherent higher quantum efficiency of photocathodes compared to photographic film, it also seems possible that the smoothing dissector, given sufficient image intensifier gain, may be able to extract more total information from an optical spectrum than can be extracted with conventional photographic recording techniques.

Our work was both encouraged and supported by the Office of Physics and Astronomy, Astronomy Programs, the National Aeronautics and Space Administration.

REFERENCES

1. U.S. Patent No. 3,355,616 (Issued 28 November, 1967).
2. Publ. Astr. Soc. of the Pacific, Vol. 82, No. 488, 837, August 1970.
3. Carnegie Institution Year Book 69, 370 (1971).
4. Rev. Sci. Instr. 31, 1246 (1960).

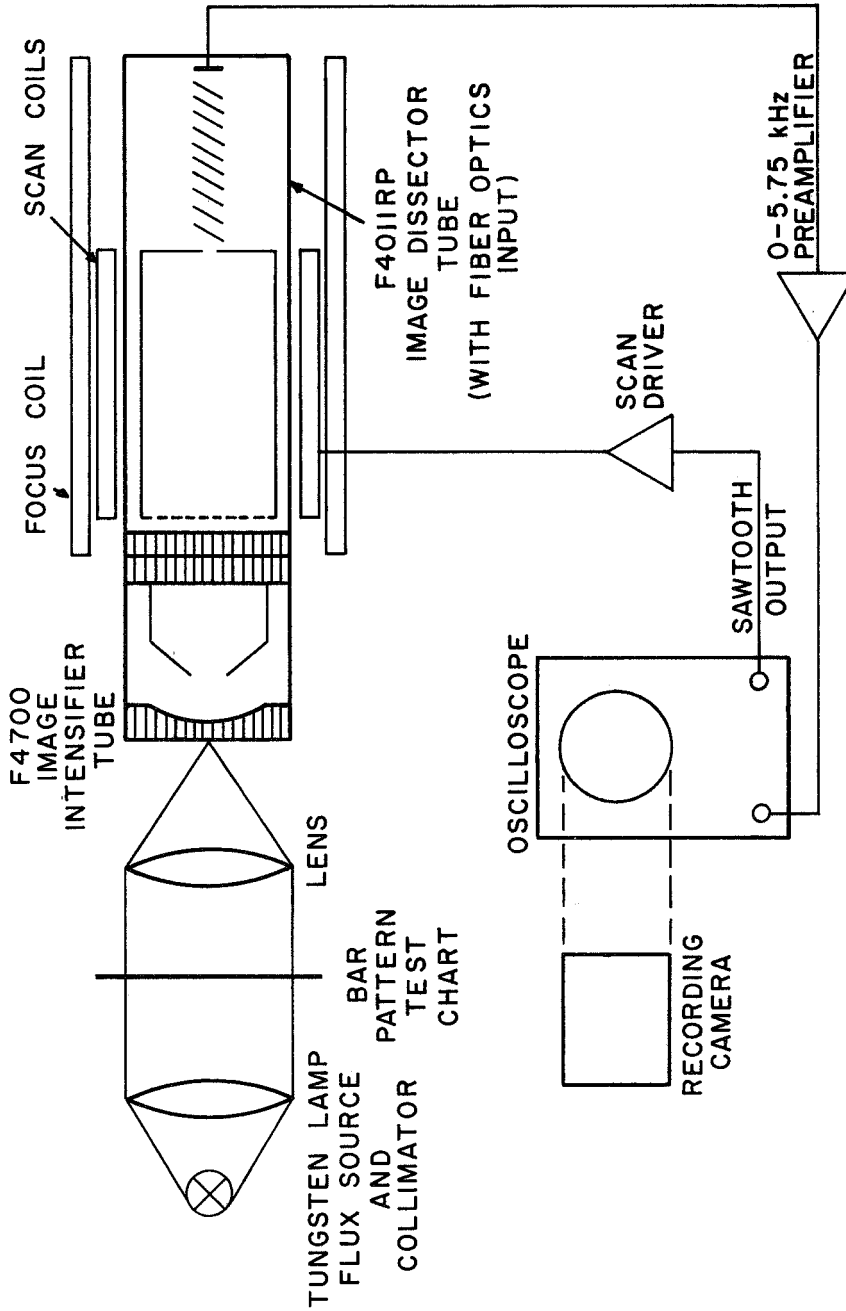
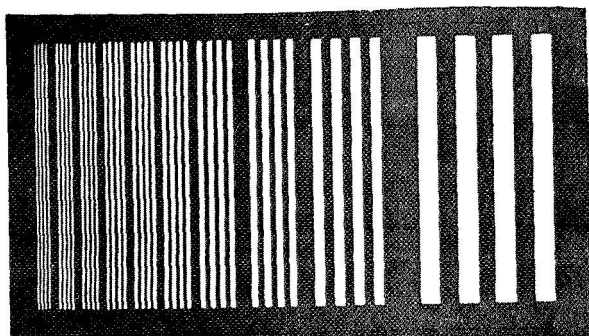


Figure 1: Basic Smoothing Dissector Configuration

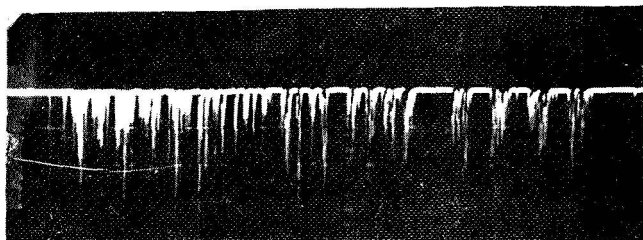


(a) Test pattern input

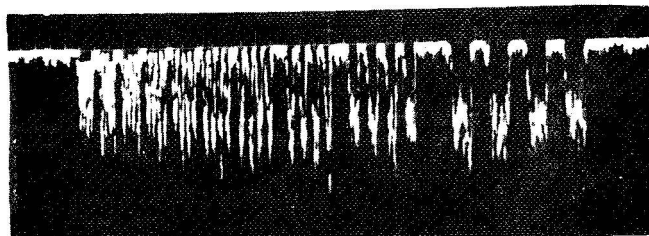


→ ← 10ms

(b) Image dissector, with smoothing



(c) Image dissector only, no smoothing, same input as (b)



(d) Image dissector only, no smoothing, 20x increase in input flux

Figure 2: Single Sweep Output Signal

(a) Simulated optical spectrum, Westinghouse ET-1332 bar pattern test chart;
 (b) Output from fiber optics F4011RP image dissector tube coupled to an F4700 image intensifier tube, 1.8×10^{10} electrons \cdot cm $^{-2}$ \cdot s $^{-1}$ highlight emission current density, oscilloscope gain: 0.5 V \cdot cm $^{-1}$; (c) output from F4011RP image dissector alone, same highlight emission current density as above, oscilloscope gain: 0.05 V \cdot cm $^{-1}$; (d) output from F4011RP image dissector alone, 20x higher flux level than (c), oscilloscope gain: 0.5 V \cdot cm $^{-1}$.

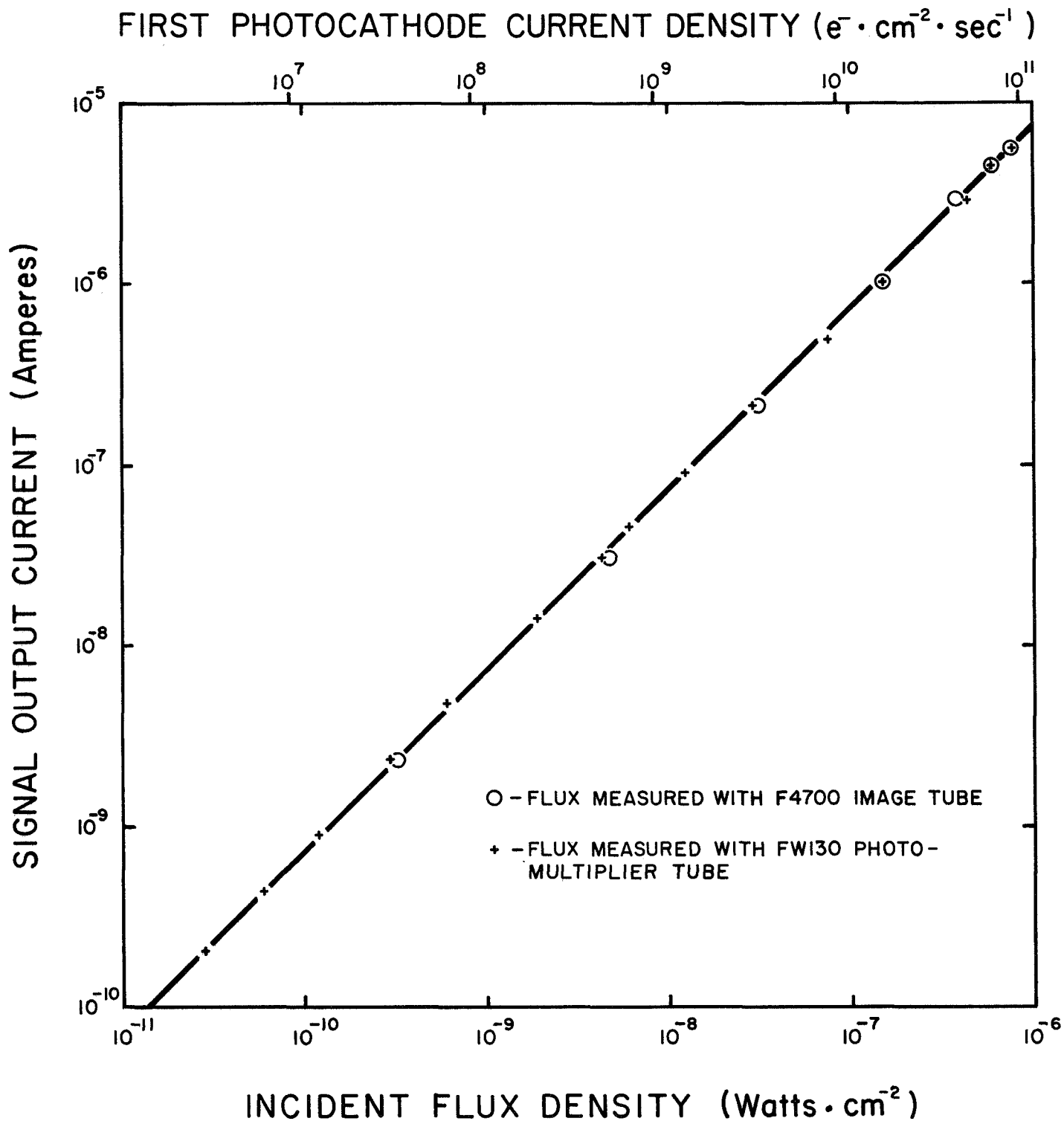


Figure 3: Measured Input/Output Linearity of an F4700/F4011RP Smoothing Dissector.
Light Source: Monsanto MV 50 650 nm GaAs light emitting diode.

APPENDIX B

This appendix contains a copy of IIT Technical Note 115,
"The Smoothing Dissector", a Novel Means of Image Scanning.

ELECTRON TUBE DIVISION
Tube and Sensor Laboratories
3700 East Pontiac Street
Fort Wayne, Indiana 46803
Telephone 219 743-7571

TECHNICAL NOTE 115

THE SMOOTHING DISSECTOR A NOVEL MEANS OF IMAGE SCANNING

When an image intensifier tube is added, as an image preamplifier, in front of an image dissector tube, interesting and potentially useful behavior results.

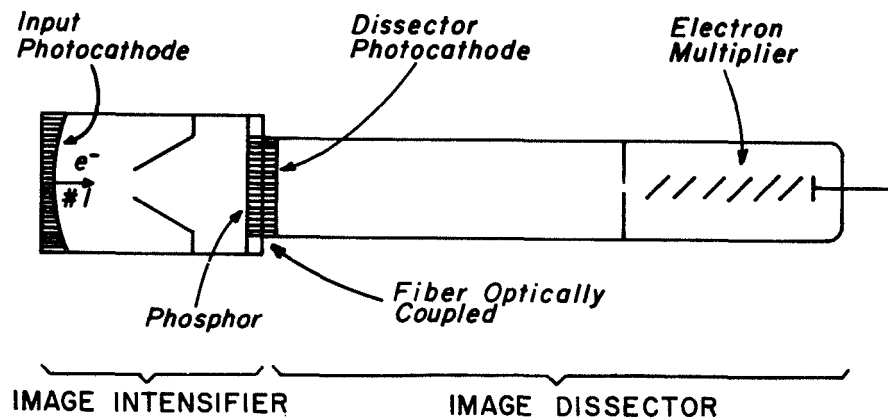


Figure 1 A Smoothing Dissector

To better understand this two-tube module, called a smoothing dissector by ITT, consider what happens to a particular photoelectron (designated as No. 1) leaving the input photocathode of the image intensifier tube. This photoelectron is accelerated to high energy (commonly 10-15 kV) and allowed to bombard a phosphor screen. This screen subsequently emits a group or chain of triggered photons (Ref. 1), usually 200-500 in number (Ref. 2) spread out in time according to the statistical time decay characteristics of the phosphor screen material. Provided that these photons are then fiber-optically coupled to the image dissector photocathode, they then excite a corresponding group of photoelectrons from the dissector photocathode, typically 30-100 in number (Refs. 3, 4).

ELECTRON TUBE DIVISION **ITT**

Two key factors are of particular significance:

(1) The triggered group of photoelectrons are not emitted simultaneously, but are spread out, time-wise, by the finite decay time characteristics of the phosphor screen(s) of the image intensifier tube. In effect, quasi-information-storage is occurring in the phosphor screen material, in terms of the temporarily excited metastable states.

(2) Each photoelectron in the triggered group contains all of the information regarding the occurrence of the triggering photoelectron (No. 1). Detection of only one of these triggered electrons is, therefore, sufficient for positive identification of the occurrence of the input photoelectron.

Since the dissector can, and does easily detect (Refs. 5, 6, 7) each individual photoelectron entering its aperture (in terms of a discrete charge pulse in its anode circuit) it now becomes possible for the dissector to detect the occurrence of the initial triggering photoelectron (No. 1) by detecting any one of the triggered group of electrons, even though this initial photoelectron event (No. 1) occurred prior to scan by the dissector aperture over the particular image element from which this electron (No. 1) was emitted. This is the fundamental principle of the smoothing dissector. It appears that some of the loss of information, "inherent" in image dissectors due to loss of all electrons emitted from an image element prior to scanning, can, in fact, be alleviated (!).

To estimate the numerical improvement possible with smoothing, consider a fast-scanned image dissector, in which the picture element dwell time, Δt defined by

$$\Delta t \equiv T/N$$

where T = time to scan a complete frame, and N = number of resolution elements per frame is considerably less than the average time interval, τ/n , between the photoelectrons making up the triggered group, where τ = decay time of the phosphor screen, and n = number of triggered electrons. This "fast-scan" restriction, namely:

$$\Delta t < \tau/n$$

minimizes the redundant statistical probability of sampling more than one of the triggered photoelectrons in one aperture dwell time, Δt .

Noting that no time correlation can exist, in general, between the sampling time, Δt , and the time of occurrence of the input photoelectron, No. 1, it can be seen from Figure 2 that the probability, $p(\text{wos})$, of detecting photoelectron No. 1 without smoothing is given by

$$p(\text{wos}) \cong \Delta t/T$$

whereas the probability, $p(\text{ws})$, with smoothing, of detecting one or more of the photoelectrons triggered by No. 1, is given by

$$p(\text{ws}) \cong n \Delta t/T = n p(\text{wos})$$

Photoelectron Emission from Intensifier Photocathode

Triggered Photoelectron Emission from Dissector Photocathode

Sampling Time

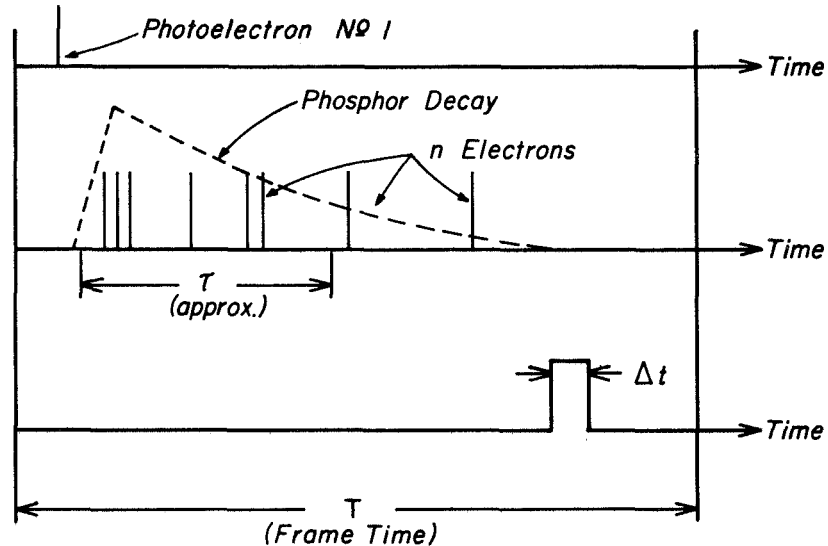


Figure 2 Detection Probability Diagram

Thus, smoothing has improved the probability of photoelectron detection by a factor of n . Since values of n from 30-50 are readily available in single stage image intensifier tubes (Ref. 4), and 1000-2000 in two stage tubes, etc., substantial improvements in the performance of image dissectors are possible by the use of smoothing.

In fact, the above reasoning leads directly to the conclusion that, for the dissector:

$$\text{Detective Quantum Efficiency (no smoothing)} \cong (\Delta t/T) Qk$$

$$\text{Detective Quantum Efficiency (with smoothing)} \cong (n \Delta t/T) Qk$$

where $Qk \cong$ quantum efficiency of the dissector photocathode = quantum efficiency available using single photomultiplier tubes for single spectral elements.

A further conclusion, based on image dissector theory (Ref. 6) is that the output signal-to-noise current ratio, SNCR (ws), with smoothing, will be related to the corresponding output signal to noise current ratio, SNCR (wos), without smoothing by:

$$\text{SNCR (ws)} \cong \sqrt{n} \text{ SNCR (wos)}$$

A restriction on the use of the preceding relationships is that fast scanning be used, such that

$$\Delta t < \tau/n \text{ where } \Delta t \equiv T/N$$

A second restriction (and this represents the true "cost" of smoothing) is that the smoothing dissector can no longer follow rapid changes in the input flux level (up to many megahertz in non-smoothing dissectors) but is limited, instead, by the slow decay time of the image intensifier phosphor screen(s) (typically a few milliseconds).

Additional studies (Refs. 8, 9, 10) of smoothing dissector behavior have been made, primarily as related to a special type of smoothing dissector called an "image dissecticon".

APPLICATIONS

One of the most promising potential applications for the smoothing dissector is for low light level spectroscopy (such as astronomical (Ref. 1) and Raman spectroscopy), where it is desired to:

- (1) Make use of the improved quantum efficiency and red response of photocathode compared to photographic film,
- (2) Eliminate cumbersome and costly banks of photomultiplier tubes,
- (3) Obtain real-time electrical readout of spectral information.
- (4) Eliminate chemical processing of photographic film, and
- (5) Eliminate the non-linearity (non-unity gamma) of photographic recording.

In this case the smoothing dissector will probably be optimized geometrically by using a slit aperture to line scan the spectral information, with the slit width selected to give the desired resolution, and the scan frequency optimized by choosing a frame time, T , approximately equal to the phosphor decay time, τ (in order to be certain of having a statistical chance of detecting every photoelectron emitted by each spectral element).

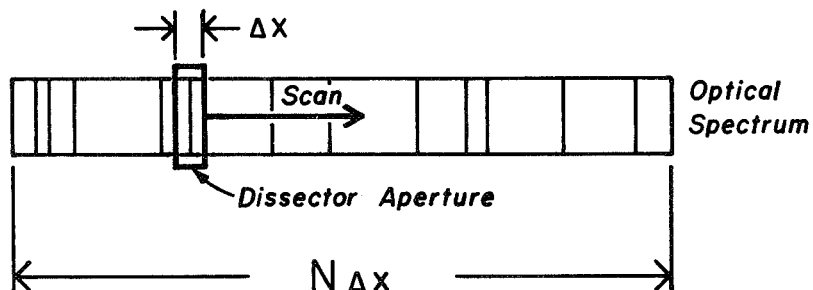


Figure 3 Spectral Scan

Thus, for line scan:

$$T \cong \tau \text{ and } \Delta t = T/N \cong \tau/N$$

This given

$$n < N$$

as the optimum smoothing condition for line scanning. This restriction, in effect, states that increasing the number of triggered photoelectrons, n (by increasing the "gain" of the pre-amplifying image intensifier) will increase the available S/N ratio only up to the point where n approaches the number of resolvable resolution elements, N . Further increase in n will only lead to redundant information extraction and no further improvement in the S/N ratio.

To maximize the S/N ratio without excessive image intensifier gain it is, therefore, probably optimum to choose

$$n \cong N$$

as the condition for optimum operation in the line scan mode. If this is indeed valid, then the earlier relationship for detective quantum efficiency reduces to:

$$\text{Detective Quantum Efficiency (Line Scan, with smoothing, } n = N) \cong Qk$$

In other words, it is possible that the smoothing line scan dissector will approach the S/N ratio capabilities of a bank of N discrete photomultiplier tubes each with a cathode quantum efficiency, Qk (!). Further analysis, and confirming experimental measurements, will be needed to determine how close the smoothing dissector can come to this maximum possible performance capability.

Figure 4 shows the measured signal-to-noise ratio characteristics of a specific smoothing dissector module, made up of an ITT F4011 Vidisector and an ITT F4714 25mm electrostatic focus, single stage image intensifier tube. The signal-to-noise ratio is plotted as a function of the noise measurement circuit bandwidth, Δf , (which is inversely proportional to the effective sampling time, Δt) in an attempt to show that smoothing is more effective for fast scan (larger Δf values). This can indeed be seen from the results shown in this figure, in terms of the wider spacing between the experimental curves for large Δf . However, an unexpected finite separation (smoothing increase) is observed even for noise measurement bandwidths as low as 10 Hz, which is well below the principal "bandwidth" of the phosphor screen (about 50-100 Hz). This apparently anomalous behavior may be due to the residual slow (tail) decay known to be present in typical phosphor screens, but until this possibility is confirmed, the results shown in Figure 4 should be treated with caution.

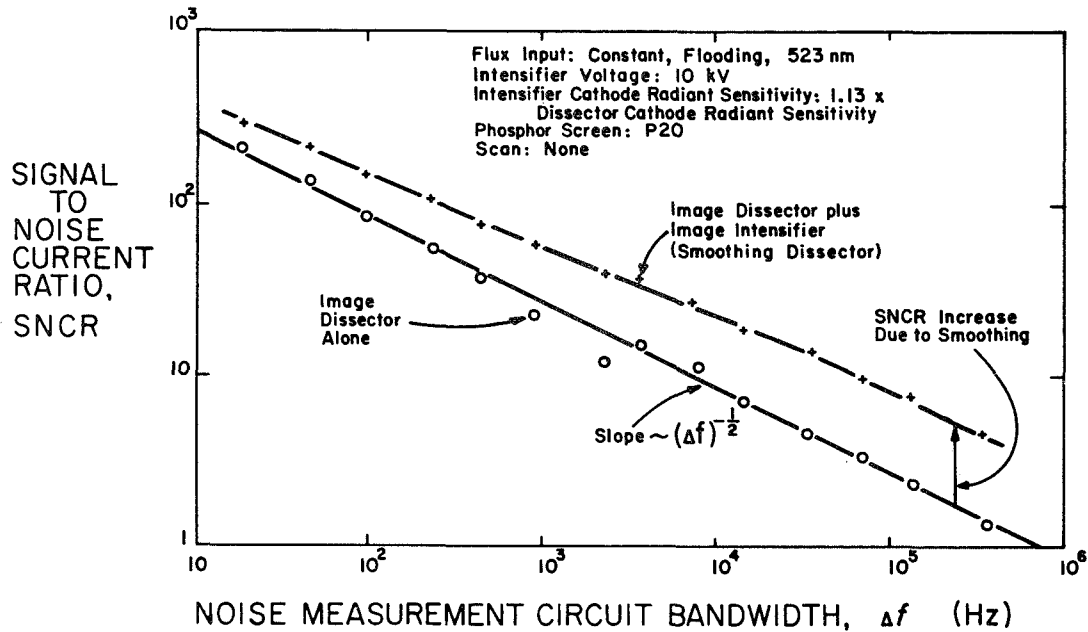


Figure 4 Measured Signal-to-Noise Current Ratio as a Function of the Noise Measurement Circuit Bandwidth for a Fiber Optics F4011 Vidisector Coupled to a 25 mm Single Stage Electro-Static Focus Image Intensifier Tube

It should be noted that since both the image intensifier tube and the image dissector are linear devices (output directly proportional to the input), the smoothing dissector should, therefore, retain this linearity and be well adapted for quantitative spectroscopy.

For further information on smoothing dissectors, the types of dissectors and image intensifiers available, and the latest experimental confirming results, contact ITT Electron Tube Division, 3700 E. Pontiac Street, Fort Wayne, Indiana 46803.

REFERENCES

1. J. McNall, L. Robinson, & E. J. Wampler: "The Response of Phosphor Output Image Intensifiers to Single Photon Inputs" (Lick Observatory, 1970) (To be published).
2. ITT Wall Chart: "Typical Absolute Spectral Response Characteristics of Aluminized Phosphor Screens" (available on request).
3. ITT Wall Chart: "Typical Absolute Spectral Response Characteristics of Photoemissive Devices" (available on request).
4. E. H. Eberhardt, Applied Optics 7, 2037 (1968).
5. E. H. Eberhardt, Applied Optics 6, 161 (1967).
6. E. H. Eberhardt, ITT Technical Note No. 101, "Signal to Noise Ratio of Image Dissectors" (1966).
7. ITT Technical Note No. 112: "A survey of Image Dissector Performance Characteristics".
8. M. Namordi: "Analysis of the Image Dissection Image Tube" ASTIA Document No. AD 639067, ARAC Document No. N67-11885, (1966).
9. W. L. Wilcock (University College of N. Wales, Bangor, Caernarvonshire, Wales): "Signal-to-Noise Analysis for Dissection Tube" (Private Communication).
10. E. H. Eberhardt: "Smoothing Electron Multipliers", ITT Research Memo 398, (1964) (available on request).

APPENDIX C

Dissector S/N Ratio

G.1 Dissector S/N Ratio (Current Measuring Mode)

The shot noise current component, i_n , of the photomission current I_{ap} entering the aperture of a dissector is given by the well known shot noise law:

$$i_n^2 = 2 e I_{ap} \Delta f$$

where "e" is the electronic charge and Δf is the effective noise bandwidth of the noise measuring circuit ($\pi/2$ times the 3 db half-power bandwidth in simple RC circuits).

This noise current is amplified by the electron multiplier, according to the gain, G, and, in addition, by an added amount given by the noise factor, k, of the electron multiplier, giving

$$(\text{anode noise current component})^2 = i_{na}^2 = G^2 k i_n^2 = 2ekG^2 I_{ap} \Delta f$$

Assuming all photocurrent to be useful signal current, an S/N current ratio, SNCR, at the anode, can then be defined as

$$\text{SNCR} = \frac{I_a}{i_{na}} = \frac{G I_{ap}}{(2ekG^2 I_{ap} \Delta f)^{1/2}} = \left(\frac{I_{ap}}{2 ek \Delta f} \right)^{1/2}$$

This is the basic S/N ratio relationship for an image dissector.

It can be re-written in terms of the input flux density, W, the cathode responsivity ratio, S, the electron transmission of the field mesh, γ (used in Vidisectors), and the aperture area, a, whose product is the aperture current, I_{ap} , giving:

$$\text{SNCR} = \left(\frac{W S \gamma a}{2ek \Delta f} \right)^{1/2}$$

The noise factor, k, which is a direct measure of the noise degradation in the electron multiplication process has a minimum value (because of the unavoidable random nature of the secondary emission process) given by

$$k_{\min} = \frac{\sigma}{\sigma - 1}$$

where $\bar{\sigma}$ = average gain/stage of the electron multiplier. Introduction of materials with higher gain/stage, such as GaP with $\bar{\sigma} \cong 30-40$, can reduce k_{\min} to a value approaching unity, i.e.

$$k_{\min} \text{ (GaP) } = 1.0$$

(However this is only a factor of about 30% improvement over conventional dynode materials, with $\bar{\sigma} = 4$, and

$$k_{\min} (\bar{\sigma} = 4) = \frac{4}{4-1} = \frac{4}{3} = 1.33)$$

The noise bandwidth, Δf , for the external circuits, must be wide enough to allow measurable signal current changes, between one image element and the next, but not too wide or reduced S/N ratio, according to the above relationships will occur. The conventional compromise here is to put the period of the noise bandwidth of the measuring circuit $1/\Delta f$ equal to 2 times the interrogation time (or sweep time) Δt for one image element:

$$1/\Delta f = 2 \Delta t$$

(This permits, for example, the interrogation of two 250 μ sec samples with a circuit bandwidth of 1kHz).

The interrogation time, Δt , can, in turn, be approximated by the ratio of the aperture dimension, s , along the direction of scan, to the scan velocity, v :

$$\Delta t = s/v$$

or by the ratio, T/n , of the time permitted, T , to scan over n resolution elements:

$$\Delta t \cong T/n$$

Thus the S/N ratio, according to the above, will be proportional to:

$$\text{SNCR} \sim (T/n)^{1/2}$$

and will be markedly reduced in magnitude if many resolution elements, n , are to be interrogated in a fixed time, T , as in detecting a spectrum of radiation.

It is this loss, by the ratio $(T/n)^{1/2}$, which the smoothing dissector is designed to reduce or eliminate.

C.2 Dissector S/N Ratio (Pulse Counting Mode)

The arrival rate of photoelectrons entering a dissector aperture, R_{ap} , is given by:

$$R_{ap} = WS \ a/e$$

where the symbols used are the same as those used above. (The quantity WS/e can be changed to the incident photon rate density, in photons/sec/cm², times the quantum efficiency of the photocathode, if so desired.)

These electrons produce a counting rate, R_a , in the anode circuit given by

$$R_a = CR_{ap}$$

where C = absolute photoelectron counting efficiency of the electron multiplier.

The total photoelectron count, N_a , at the anode in a counting time, t , is then given by:

$$N_a = R_a \Delta t = CWS \gamma_a \Delta t/e$$

This count will be subjected to an unavoidable statistical variance (assuming random emission of electrons) given by:

$$\text{variance} = \pm (CWS \gamma_a \Delta t/e)^{1/2}$$

Since the dark count rate of most small aperture dissectors is negligible compared to N_a , this signal count variance represents essentially the sole source of "noise" for the dissector in this counting mode of operation. An S/N ratio can then be expressed as

$$\text{SNCR} = \frac{\text{signal count}}{\text{variance}} = (CWS \gamma_a \Delta t/e)^{1/2}$$

Comparison of this result (for the counting mode) with the previous result (for the current measuring mode) shows that the two are exactly equivalent for:

$$t = 1/2 \Delta f$$

(as previously approximated), and if the counting efficiency, C , were related to the noise factor, k , according to

$$C = 1/k$$

A principle advantage of the counting mode of operation is that it is experimentally easier to achieve high values of the counting efficiency, C , (approaching unity) than it is to achieve low values of the noise factor, k (also approaching unity). Experimentally, the magnitude of the counting efficiency C depends on the bias discriminator level setting in the counting circuits, which must be selected with care. However, for image dissectors (whose apertures are inherently small), the spurious small-amplitude dark count can be kept small, by proper tube design, permitting counting efficiencies approaching unity (100%) to be achieved. This is a (sometimes hidden) advantage of the smoothing dissector over competitive devices, such as banks of photomultiplier tubes.